Exact Potts Model Partition Function on Strips of the Triangular Lattice

Shu-Chiuan Chang[(a)*] and Robert Shrock[(a,b)**]

(a) C. N. Yang Institute for Theoretical Physics
State University of New York
Stony Brook, N. Y. 11794-3840
(b) Physics Department
Brookhaven National Laboratory
Upton, NY 11973

Abstract

In this paper we present exact calculations of the partition function Z of the q-state Potts model and its generalization to real q, for arbitrary temperature on n-vertex strip graphs, of width $L_y = 2$ and arbitrary length, of the triangular lattice with free, cyclic, and Möbius longitudinal boundary conditions. These partition functions are equivalent to Tutte/Whitney polynomials for these graphs. The free energy is calculated exactly for the infinite-length limit of the graphs, and the thermodynamics is discussed. Considering the full generalization to arbitrary complex q and temperature, we determine the singular locus $\mathcal{B}$ in the corresponding $\mathbb{C}^2$ space, arising as the accumulation set of partition function zeros as $n \to \infty$. In particular, we study the connection with the $T = 0$ limit of the Potts antiferromagnet where $\mathcal{B}$ reduces to the accumulation set of chromatic zeros. Comparisons are made with our previous exact calculation of Potts model partition functions for the corresponding strips of the square lattice. Our present calculations yield, as special cases, several quantities of graph-theoretic interest.

*email: shu-chiuan.chang@sunysb.edu
**(a): permanent address; email: robert.shrock@sunysb.edu

1 Introduction

The q-state Potts model has served as a valuable model for the study of phase transitions and critical phenomena [1, 2]. On a lattice, or, more generally, on a (connected) graph G, at temperature T, this model is defined by the partition function

$$Z(G,q,v) = \sum_{\{\sigma_n\}} e^{-\beta \mathcal{H}} \tag{1.1}$$

with the (zero-field) Hamiltonian

$$\mathcal{H} = -J \sum_{\langle ij \rangle} \delta_{\sigma_i \sigma_j} \tag{1.2}$$

where $\sigma_i = 1, ..., q$ are the spin variables on each vertex $i \in G$; $\beta = (k_B T)^{-1}$; and $\langle ij \rangle$ denotes pairs of adjacent vertices. The graph $G = G(V, E)$ is defined by its vertex set V and its edge set E; we denote the number of vertices of G as $n = n(G) = |V|$ and the number of edges of G as $e(G) = |E|$. We use the notation

$$K = \beta J \ , \quad a = u^{-1} = e^K \ , \quad v = a - 1 \tag{1.3}$$

so that the physical ranges are (i) $a \ge 1$, i.e., $v \ge 0$ corresponding to $\infty \ge T \ge 0$ for the Potts ferromagnet, and (ii) $0 \le a \le 1$, i.e., $-1 \le v \le 0$, corresponding to $0 \le T \le \infty$ for the Potts antiferromagnet. One defines the (reduced) free energy per site $f = -\beta F$, where F is the actual free energy, via

$$f(\{G\}, q, v) = \lim_{n \to \infty} \ln[Z(G,q,v)^{1/n}] \ . \tag{1.4}$$

where we use the symbol $\{G\}$ to denote $\lim_{n\to\infty} G$ for a given family of graphs.

Let $G' = (V, E')$ be a spanning subgraph of G, i.e. a subgraph having the same vertex set V and an edge set $E' \subseteq E$. Then $Z(G,q,v)$ can be written as the sum [3]-[5]

$$\begin{aligned} Z(G,q,v) &= \sum_{G' \subseteq G} q^{k(G')} v^{e(G')} \\ &= \sum_{r=k(G)}^{n(G)} \sum_{s=0}^{e(G)} z_{rs} q^r v^s \end{aligned} \tag{1.5}$$

where $k(G')$ denotes the number of connected components of G' and $z_{rs} \ge 0$. Since we only consider connected graphs G, we have $k(G) = 1$. The formula (1.5) enables one to generalize q from $\mathbb{Z}_+$ to $\mathbb{R}_+$ (keeping v in its physical range). This generalization is sometimes denoted the random cluster model [5]; here we shall use the term "Potts model" to include both positive integral q as in the original formulation in eqs. (1.1) and (1.2), and the generalization to real (or complex) q, via eq. (1.5). The formula (1.5) shows that $Z(G,q,v)$ is a polynomial in q and v (equivalently, a) with maximum and minimum degrees indicated in eq. (1.5). The Potts model partition function on a graph G is essentially equivalent to the Tutte polynomial [6]-[8] and Whitney rank polynomial [4], [2], [9]-[11] for this graph, as discussed in the appendix.

In this paper we shall present exact calculations of the Potts model partition function for strips of the triangular lattice of width $L_y = 2$ vertices (or equivalently edges) and arbitrary length L_x with various boundary conditions. This is a natural continuation of a previous study by one of us of the Potts model model on the analogous strips of the square lattice [12, 13], and the reader is referred to that paper for

background and further references. We envision the strip of the triangular lattice as being formed by starting with a ladder graph, i.e. $2 \times L_x$ strip of the square lattice, and then adding edges joining, say, the lower left and upper right vertices of each square. The longitudinal (transverse) direction is taken as the horizontal, x (vertical, y) direction. We use free transverse boundary conditions and consider free, periodic (= cyclic), and Möbius longitudinal boundary conditions. These families of graphs are denoted, respectively, as S_m (for open strip), L_m (for ladder), and ML_m (for Möbius ladder), where $L_x = m+1$ (edges) for S_m (following our labelling convention in [26]) and $L_x = m$ for L_m and ML_m. One has $n(S_m) = 2(m+2)$ and $n(L_m) = n(ML_m) = 2m$. Each vertex on the cyclic strip L_m has degree (coordination number) $\Delta = 4$; this is also true of the interior vertices on the open strip S_m. The Möbius strip can involve a seam, as discussed in [14].

The motivations for these exact calculations of Potts model partition functions for strips of various lattices were discussed in [13]. Clearly, new exact calculations of Potts model partition functions are of value in their own right. In addition, it was shown [13] that these calculations can give insight into the complex-temperature phase diagram of the 2D Potts model on the given lattice. This is useful, since the 2D Potts model has never been solved except in the $q = 2$ Ising case. Furthermore, with these exact results one can study both the $T = 0$ critical point of the q-state Potts ferromagnet and, for certain q values ($q = 2$ for the square strip; $q = 2, 3$ for the present strip of the triangular lattice) the $T = 0$ critical point of the Potts antiferromagnet. In addition, via the correspondence with the Tutte polynomial, our calculations yield several quantities of relevance to mathematical graph theory.

Various special cases of the Potts model partition function are of interest. One special case is the zero-temperature limit of the Potts antiferromagnet (AF). For sufficiently large q, on a given lattice or graph G, this exhibits nonzero ground state entropy (without frustration). This is equivalent to a ground state degeneracy per site (vertex), $W > 1$, since $S_0 = k_B \ln W$. The $T = 0$ (i.e., $v = -1$) partition function of the above-mentioned q-state Potts antiferromagnet (PAF) on G satisfies

$$Z(G, q, -1) = P(G, q) \tag{1.6}$$

where $P(G, q)$ is the chromatic polynomial (in q) expressing the number of ways of coloring the vertices of the graph G with q colors such that no two adjacent vertices have the same color [3, 9, 15, 16]. The minimum number of colors necessary for this coloring is the chromatic number of G, denoted $\chi(G)$. We have

$$W(\{G\}, q) = \lim_{n \to \infty} P(G, q)^{1/n} \tag{1.7}$$

Using the formula (1.5) for $Z(G, q, v)$, one can generalize q from $\mathbb{Z}_+$ not just to $\mathbb{R}_+$ but to $\mathbb{C}$ and a from its physical ferromagnetic and antiferromagnetic ranges $1 \le a \le \infty$ and $0 \le a \le 1$ to $a \in \mathbb{C}$. A subset of the zeros of Z in the two-complex dimensional space $\mathbb{C}^2$ defined by the pair of variables (q, a) can form an accumulation set in the $n \to \infty$ limit, denoted $\mathcal{B}$, which is the continuous locus of points where the free energy is nonanalytic. This locus is determined as the solution to a certain $\{G\}$-dependent equation [12, 13]. For a given value of a, one can consider this locus in the q plane, and we denote it as $\mathcal{B}_q(\{G\}, a)$. In the special case $a = 0$ (i.e., $v = -1$) where the partition function is equal to the chromatic polynomial, the zeros in q are the chromatic zeros, and $\mathcal{B}_q(\{G\}, a = 0)$ is their continuous accumulation set in the $n \to \infty$ limit [15]-[14]. In a series of papers we have given exact calculations of the chromatic polynomials and nonanalytic loci $\mathcal{B}_q$ for various families of graphs (for further references on this $a = 0$ special case, see [13]). With the exact Potts partition function for arbitrary temperature, one can study $\mathcal{B}_q$ for $a \neq 0$ and, for a given value of q, one can study the continuous accumulation set of the zeros of $Z(G, q, v)$ in the a plane; this will be

denoted $\mathcal{B}_a(\{G\},q)$. It will often be convenient to consider the equivalent locus in the $u=1/a$ plane, namely $\mathcal{B}_u(\{G\},q)$. We shall sometimes write $\mathcal{B}_q(\{G\},a)$ simply as $\mathcal{B}_q$ when $\{G\}$ and a are clear from the context, and similarly with $\mathcal{B}_a$ and $\mathcal{B}_u$. One gains a unified understanding of the separate loci $\mathcal{B}_q(\{G\})$ for fixed a and $\mathcal{B}_a(\{G\})$ for fixed q by relating these as different slices of the locus $\mathcal{B}$ in the $\mathbb{C}^2$ space defined by (q,a) as we shall do here.

Following the notation in [17] and our other earlier works on $\mathcal{B}_q(\{G\})$ for $a=0$, we denote the maximal region in the complex q plane to which one can analytically continue the function $W(\{G\},q)$ from physical values where there is nonzero ground state entropy as R_1 . The maximal value of q where $\mathcal{B}_q$ intersects the (positive) real axis was labelled $q_c(\{G\})$. Thus, region R_1 includes the positive real axis for $q > q_c(\{G\})$. Correspondingly, in our works on complex-temperature properties of spin models, we had labelled the complex-temperature extension (CTE) of the physical paramagnetic phase as (CTE)PM, which will simply be denoted PM here, the extension being understood, and similarly with ferromagnetic (FM) and antiferromagnetic (AFM); other complex-temperature phases, having no overlap with any physical phase, were denoted O_j (for "other"), with j indexing the particular phase [39]. Here we shall continue to use this notation for the respective slices of $\mathcal{B}$ in the q and a or u planes.

We record some special values of $Z(G,q,v)$ below, beginning with the $q=0$ special case

$$Z(G,0,v) = 0 \tag{1.8}$$

which implies that $Z(G,q,v)$ has an overall factor of q. In general (and for all the graphs considered here), this is the only overall factor that it has. We also have

$$Z(G,1,v) = \sum_{G' \subseteq G} v^{e(G')} = a^{e(G)} \ . \tag{1.9}$$

For temperature $T=\infty$, i.e., $v=0$,

$$Z(G,q,0) = q^{n(G)} \ . \tag{1.10}$$

Further,

$$Z(G,q,-1) = P(G,q) = \Big[\prod_{s=0}^{\chi(G)-1} (q-s) \Big] U(G,q) \tag{1.11}$$

where $U(G,q)$ is a polynomial in q of degree $n(G)-\chi(G)$.

We note some values of chromatic numbers for the strip graphs considered here:

$$\chi(S_m) = 3 \tag{1.12}$$

$$\chi(L_m) = \begin{cases} 3 & \text{if } m = 0 \mod 3 \\ 4 & \text{if } m = 1 \text{ or } m = 2 \mod 3 \end{cases} \tag{1.13}$$

and

$$\chi(ML_m) = 4 \ . \tag{1.14}$$

Hence, for $q = 1,2,3$ we have

$$Z(G,q,-1) = P(G,q) = 0 \quad \text{for} \quad G = S_m,\ L_m,\ ML_m \quad \text{and} \quad q = 1,2 \tag{1.15}$$

$$Z(G,3,-1) = P(G,3) = 3! \quad \text{for} \quad G = S_m \ \text{ or } \ G = L_{m=0 \ mod \ 3} \tag{1.16}$$

where $G = L_{m=0 \ mod \ 3}$ means that this applies to L_m for $m = 0$ mod 3. For the graphs $G = S_m, L_m$, and ML_m, (i) the result (1.15) implies that for $q=2$, $Z(G,2,v)$ contains at least one power of the factor

$(v+1) = a$; for $q = 1$, one already knows the form of $Z(G, 1, v)$ from (1.9); (ii) the result (1.16) implies that for the cases where $\chi(G) = 4$, $Z(G, 3, v)$ contains at least one power of $(v + 1)$ as a factor.

Another basic property, evident from eq. (1.5), is that (i) the zeros of $Z(G, q, v)$ in q for real v and hence also the continuous accumulation set $\mathcal{B}_q$ are invariant under the complex conjugation $q \to q^*$; (ii) the zeros of $Z(G, q, v)$ in v or equivalently a for real q and hence also the continuous accumulation set $\mathcal{B}_a$ are invariant under the complex conjugation $a \to a^*$.

Just as the importance of noncommutative limits was shown in (eq. (1.9) of) [17] on chromatic polynomials, so also one encounters an analogous noncommutativity here for the general partition function (1.5) of the Potts model for nonintegral q: at certain special points q_s (typically $q_s = 0, 1..., \chi(G)$) one has

$$\lim_{n\to\infty} \lim_{q\to q_s} Z(G, q, v)^{1/n} \ne \lim_{q\to q_s} \lim_{n\to\infty} Z(G, q, v)^{1/n} \ . \tag{1.17}$$

Because of this noncommutativity, the formal definition (1.4) is, in general, insufficient to define the free energy f at these special points q_s; it is necessary to specify the order of the limits that one uses in eq. (1.17). We denote the two definitions using different orders of limits as f_{qn} and f_{nq}:

$$f_{nq}(\{G\}, q, v) = \lim_{n\to\infty} \lim_{q\to q_s} n^{-1} \ln Z(G, q, v) \tag{1.18}$$

$$f_{qn}(\{G\}, q, v) = \lim_{q\to q_s} \lim_{n\to\infty} n^{-1} \ln Z(G, q, v) \ . \tag{1.19}$$

In Ref. [17] and our subsequent works on chromatic polynomials and the above-mentioned zero-temperature antiferromagnetic limit, it was convenient to use the ordering $W(\{G\}, q_s) = \lim_{q\to q_s} \lim_{n\to\infty} P(G, q)^{1/n}$ since this avoids certain discontinuities in W that would be present with the opposite order of limits. In the present work on the full temperature-dependent Potts model partition function, we shall consider both orders of limits and comment on the differences where appropriate. Of course in discussions of the usual q-state Potts model (with positive integer q), one automatically uses the definition in eq. (1.1) with (1.2) and no issue of orders of limits arises, as it does in the Potts model with real q.

As a consequence of the noncommutativity (1.17), it follows that for the special set of points $q = q_s$ one must distinguish between (i) $(\mathcal{B}_a(\{G\}, q_s))_{nq}$, the continuous accumulation set of the zeros of $Z(G, q, v)$ obtained by first setting $q = q_s$ and then taking $n \to \infty$, and (ii) $(\mathcal{B}_a(\{G\}, q_s))_{qn}$, the continuous accumulation set of the zeros of $Z(G, q, v)$ obtained by first taking $n \to \infty$, and then taking $q \to q_s$. For these special points,

$$(\mathcal{B}_a(\{G\}, q_s))_{nq} \ne (\mathcal{B}_a(\{G\}, q_s))_{qn} \ . \tag{1.20}$$

From eq. (1.8), it follows that for any G,

$$\exp(f_{nq}) = 0 \quad \text{for} \quad q = 0 \tag{1.21}$$

and thus

$$(\mathcal{B}_a)_{nq} = \emptyset \quad \text{for} \quad q = 0 \ . \tag{1.22}$$

However, for many families of graphs, including the circuit graph C_n, and cyclic and Möbius strips of the square or triangular lattice, if we take $n \to \infty$ first and then $q \to 0$, we find that $(\mathcal{B}_u)_{qn}$ is nontrivial. Similarly, from (1.9) we have, for any G,

$$(\mathcal{B}_a)_{nq} = \emptyset \quad \text{for} \quad q = 1 \tag{1.23}$$

since all of the zeros of Z occur at the single discrete point $a = 0$ (and in the case of a graph G with no edges, $Z = 1$ with no zeros). However, as the simple case of the circuit graph shows [13], $(\mathcal{B}_u)_{qn}$ is, in general, nontrivial.

As derived in [13], a general form for the Potts model partition function for the strip graphs considered here, or more generally, for recursively defined families of graphs comprised of m repeated subunits (e.g. the columns of squares of height L_y vertices that are repeated L_x times to form an $L_x \times L_y$ strip of a regular lattice with some specified boundary conditions), is

$$Z(G, q, v) = \sum_{j=1}^{N_\lambda} c_{G,j} (\lambda_{G,j}(q, v))^m \tag{1.24}$$

where N_λ depends on G.

The Potts ferromagnet has a zero-temperature phase transition in the $L_x \to \infty$ limit of the strip graphs considered here, and this has the consequence that for cyclic and Möbius boundary conditions, $\mathcal{B}$ passes through the $T = 0$ point $u = 0$. It follows that $\mathcal{B}$ is noncompact in the a plane. Hence, it is usually more convenient to study the slice of $\mathcal{B}$ in the $u = 1/a$ plane rather than the a plane. Since $a \to \infty$ as $T \to 0$ and Z diverges like $a^{e(G)}$ in this limit, we shall use the reduced partition function Z_r defined by

$$Z_r(G, q, v) = a^{-e(G)} Z(G, q, v) = u^{e(G)} Z(G, q, v) \tag{1.25}$$

which has the finite limit $Z_r \to 1$ as $T \to 0$. For a general strip graph $(G_s)_m$ of type G_s and length $L_x = m$, we can write

$$Z_r((G_s)_m, q, v) \quad = \quad u^{e((G_s)_m)} \sum_{j=1}^{N_\lambda} c_{G_s,j} (\lambda_{G_s,j})^m \equiv \sum_{j=1}^{N_\lambda} c_{G_s,j} (\lambda_{G_s,j,u})^m \tag{1.26}$$

with

$$\lambda_{G_s,j,u} = u^{e((G_s)_m)/m} \lambda_{G_s,j} \ . \tag{1.27}$$

For example, for the $L_y = 2$ strips of the triangular lattice of interest here, with free transverse boundary conditions and either free or periodic longitudinal boundary conditions, we have $e(S_m) = 4m + 5$ and $e(L_m) = 4m$. (In the case of the cyclic strip with $m = 2$, L_m degenerates in the sense that it contains multiple edges connecting some pairs of vertices, and similarly, for $m = 1$, L_m contains both multiple edges and loops; the above formula applies to these cases if one takes care to count these multiple edges and loops, as is discussed further below.)

2 Strip of Triangular Lattice with Free Longitudinal Boundary Conditions

In this section we present the Potts model partition function $Z(S_m, q, v)$ for the $L_y = 2$ strip of the triangular lattice S_m with arbitrary length $L_x = m + 1$ (i.e., containing $m + 1$ squares) and free transverse and longitudinal boundary conditions. One convenient way to express the results is in terms of a generating function:

$$\Gamma(S, q, v, z) = \sum_{m=0}^{\infty} Z(S_m, q, v) z^m \ . \tag{2.1}$$

We have calculated this generating function using the deletion-contraction theorem for the corresponding Tutte polynomial $T(S_m, x, y)$ and then expressing the result in terms of the variables q and v. We find

$$\Gamma(S, q, v, z) = \frac{\mathcal{N}(S, q, v, z)}{\mathcal{D}(S, q, v, z)} \tag{2.2}$$

where

$$\mathcal{N}(S, q, v, z) = A_{S,0} + A_{S,1} z \tag{2.3}$$

with

$$A_{S,0} = q(v^5 + 5v^4 + 8v^3 + 2v^3 q + 10v^2 q + 5vq^2 + q^3) \tag{2.4}$$

$$A_{S,1} = -q(v+1)^2 (v+q)^3 v^2 \tag{2.5}$$

and

$$\mathcal{D}(S, q, v, z) = 1 - (v^4 + 4v^3 + 7v^2 + 4qv + q^2)z + (v+1)^2 (v+q)^2 v^2 z^2 \ . \tag{2.6}$$

(The generating function for the Tutte polynomial $T(S_m, x, y)$ is given in the appendix.) Writing

$$\mathcal{D}(S, q, v, z) = \prod_{j=1}^{2} (1 - \lambda_{S,j} z) \tag{2.7}$$

we have

$$\lambda_{S,(1,2)} = \frac{1}{2}\left[T_{S12} \pm (3v + v^2 + q)\sqrt{R_{S12}} \ \right] \tag{2.8}$$

where

$$T_{S12} = v^4 + 4v^3 + 7v^2 + 4qv + q^2 \tag{2.9}$$

and

$$R_{S12} = q^2 + 2qv - 2qv^2 + 5v^2 + 2v^3 + v^4 \ . \tag{2.10}$$

Ref. [28] presented a formula to obtain the chromatic polynomial for a recursive family of graphs in the form of sums of powers of λ_j's starting from the generating function, and the generalization of this to the full Potts model partition function was given in [13]. Using this, we have

$$Z(S_m, q, v) = \frac{(A_{S,0}\lambda_{S,1} + A_{S,1})}{(\lambda_{S,1} - \lambda_{S,2})} \lambda_{S,1}^m + \frac{(A_{S,0}\lambda_{S,2} + A_{S,1})}{(\lambda_{S,2} - \lambda_{S,1})} \lambda_{S,2}^m \tag{2.11}$$

(which is symmetric under $\lambda_{S,1} \leftrightarrow \lambda_{S,2}$). Although both the $\lambda_{S,j}$'s and the coefficient functions involve the square root $\sqrt{R_{S12}}$ and are not polynomials in q and v, the theorem on symmetric functions of the roots of an algebraic equation [40] guarantees that $Z(S_m, q, v)$ is a polynomial in q and v (as it must be by (1.5) since the coefficients of the powers of z in the equation (2.6) defining these $\lambda_{S,j}$'s are polynomials in these variables q and v.

As will be shown below, for $q \ge 2$ (and for $0 \le q < 1$, with the f_{qn} and $(\mathcal{B}_u)_{qn}$ definitions) the singular locus $\mathcal{B}_u$ for this strip consists of arcs that do not separate the u plane into different regions, so that the PM phase and its complex-temperature extension occupy all of this plane, except for these arcs. For these ranges of q, the (reduced) free energy is given by

$$f = \frac{1}{2} \ln \lambda_{S,1} \ . \tag{2.12}$$

This is analytic for all finite temperature, for both the ferromagnetic and antiferromagnetic sign of the spin-spin coupling J. The internal energy and specific heat can be calculated in a straightforward manner from the free energy (2.12); since the resultant expressions are somewhat cumbersome, we do not list them here. In contrast, for the range $1 < q < 2$, the Potts antiferromagnet on the $L_x \to \infty$ limit of this open strip does have a phase transition at finite temperature (see eq. (2.2.6)), but this has unphysical features, including a specific heat and partition function Z that are negative for some range of temperature, and non-existence of a thermodynamic limit independent of boundary conditions. This will be discussed further below.

We next consider the limits of zero temperature for the antiferromagnetic and ferromagnetic cases. Let us define

$$D_k(q) = \frac{P(C_k,q)}{q(q-1)} = \sum_{s=0}^{k-2} (-1)^s \binom{k-1}{s} q^{k-2-s} \tag{2.13}$$

and $P(C_k,q)$ is the chromatic polynomial for the circuit (cyclic) graph C_k with k vertices,

$$P(C_k,q) = (q-1)^k + (q-1)(-1)^k \tag{2.14}$$

so that $D_2 = 1$, $D_3 = q-2$, $D_4 = q^2-3q+3$, and so forth for other D_k's. In the $T = 0$ Potts antiferromagnet limit $v = -1$, $\lambda_{S,1} = D_3^2 = (q-2)^2$ and $\lambda_{S,2} = 0$, so that eq. (2.2) reduces to the generating function for the chromatic polynomial for this open strip

$$\Gamma(S,q,-1;z) = \frac{q(q-1)(q-2)^2}{1-(q-2)^2 z} \tag{2.15}$$

Equivalently, the chromatic polynomial is

$$P(S_m,q) = q(q-1)(q-2)^{2(m+1)} \ . \tag{2.16}$$

For the ferromagnetic case with general q, in the low-temperature limit $v \to \infty$,

$$\lambda_{S,1} = v^4 + 4v^3 + O(v^2) \ , \quad \lambda_{S,2} = v^2 + 2(q-1)v + O(1) \quad \text{as} \quad v \to \infty \tag{2.17}$$

so that $|\lambda_{S,1}|$ is never equal to $|\lambda_{S,2}|$ in this limit, and hence $\mathcal{B}_u$ does not pass through the origin of the u plane for the $n \to \infty$ limit of the open square strip:

$$u = 0 \notin \mathcal{B}_u(\{S\}). \tag{2.18}$$

In contrast, as will be shown below, $\mathcal{B}_u$ does pass through $u = 0$ for this strip with cyclic or Möbius boundary conditions.

2.1 $\mathcal{B}_q(\{S\})$ for fixed a

We start with the value $a = 0$ corresponding to the Potts antiferromagnet at zero temperature. In this case, $Z(S_m,q,v=-1) = P(S_m,q)$, where this chromatic polynomial was given in eq. (2.16), and the continuous locus $\mathcal{B}_q = \emptyset$. For a in the finite-temperature antiferromagnetic range $0 < a < 1$, $\mathcal{B}_q$ consists of a single self-conjugate arc crossing the positive real q axis at

$$q_c(\{S\}) = -v(3+v) = (1-a)(2+a) \tag{2.1.1}$$

where the factor $(3v+v^2+q)$ multiplying the square root in eq. (2.8) vanishes, so that the two roots coincide. Parenthetically, we observe that this is same as the value of q_c for the Potts model on the $n \to \infty$ limit of

the circuit graph, C_n [12, 13]. The arc endpoints occur at the branch points where the square root is zero, viz.,

$$q_{S,endpt.} = (a-1)[a - 2 \pm 2i\sqrt{a}\ ] \ . \tag{2.1.2}$$

As a increases from 0 to 1, the crossing point (2.1.1) decreases monotonically from 2 to 0, and as a reaches the infinite-temperature value 1, $\mathcal{B}_q$ shrinks to a point at the origin. In the ferromagnetic range $a > 1$ the self-conjugate arc crosses the negative real axis, since $q_c(\{S\}) < 0$, and has support in the $Re(q) < 0$ half-plane. In Figs. 1 and 2 we show $\mathcal{B}_q$ and associated zeros of Z in the q plane for the antiferromagnetic value $a = 0.1$ and the ferromagnetic value $a = 2$.

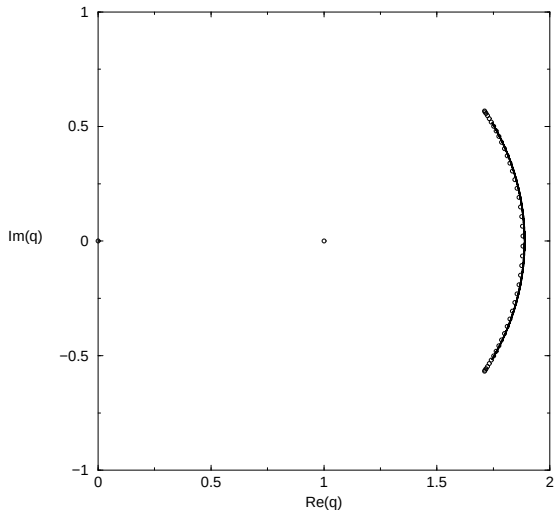

Figure 1: Locus $\mathcal{B}_q$ for the $n \to \infty$ limit of the $L_y = 2$ triangular strip $\{S\}$ with free longitudinal boundary conditions, for $a = 0.1$. Zeros of $Z(S_m, q, v = -0.9)$ for $m = 20$ (i.e., $n = 44$ vertices, so that Z is a polynomial of degree 44 in q) are shown for comparison.

2.2 $\mathcal{B}_u$ for fixed q

We show several plots of the locus $\mathcal{B}_u$ for various values of q in Figs. 3 - 8. For values of q where non-commutativity occurs, we consider $\mathcal{B}_{qn}$. Given the algebraic structure of $\lambda_{S,j}$, $j = 1, 2$, the degeneracy of magnitudes $|\lambda_{S,1}| = |\lambda_{S,2}|$ and hence the locus $\mathcal{B}_u$ occurs where (i) $T_{S12} = 0$, (ii) the prefactor of the square root vanishes: $3v + v^2 + q = 0$, (iii) $R_{S12} = 0$, (iv) if q is real, where $R_{S12} < 0$ so that the square root is pure imaginary, and (v) elsewhere for complex u, where the degeneracy condition is satisfied. All of these five possibilities are realized here, although some, such as (i) can yield solutions already subsumed by other conditions; for example, for the case $q = 1.8$, shown in Fig. 5, T_{S12} vanishes at two real points, $u \simeq -29.1,\ -1.35$, both of which are subsumed within the solution of condition (iv), which is a line segment $-69.486 < u < -1.291$, and so forth for various other solutions. In cases where $\mathcal{B}_u$ does not enclose regions, $\lambda_{S,1}$ is dominant everywhere in the u plane, and degenerate in magnitude with $\lambda_{S,2}$ on $\mathcal{B}_u$; the cases where $\mathcal{B}_u$ does enclose regions will be discussed individually.

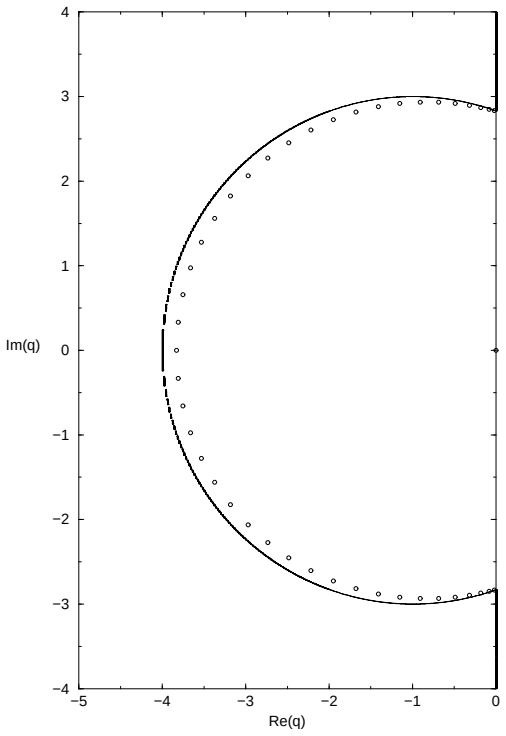

Figure 2: Locus $\mathcal{B}_q$: same as Fig. 1 for $a = 2$ (i.e., $v = 1$).

For large values of q, we find that $\mathcal{B}_u$ consists of the union of (i) a circular arc centered at $u \sim -1/q$ that crosses the negative real u axis, and (ii) a line segment on the negative u axis. For example, for $q = 10$, the arc has its endpoints at two of the branch point zeros of $\sqrt{R_{S12}}$, at $u = (7 \pm \sqrt{15}i)/32 \simeq 0.21875 \pm 0.12103i$, and the line segment, which is the solution to the condition (iv) above, that $R_{S12} < 0$ for real q, has left and right endpoints at $u_1 = -1$ and $u_2 = -1/4$. As q decreases, u_1 and u_2 move toward more negative values, and as q decreases to 2, $u_1 \to -\infty$, i.e. $a = 0$, while $u_2 \to -1$. For $q = 2$, $\mathcal{B}_u$ is the union of the above line segment $-\infty < u < -1$ and the circular arc

$$u = -1 + \sqrt{2}e^{\pm i\theta} \ , \quad \theta_e \le \theta \le \pi \tag{2.2.1}$$

where

$$\theta_e = arctan\Big(\frac{\sqrt{7}}{11}\Big) \simeq 13.5^\circ \ . \tag{2.2.2}$$

That is, the endpoints of the circular arc occur at

$$u_e = \frac{1}{8}(3 \pm \sqrt{7}\ i) \tag{2.2.3}$$

Proceeding, we observe that for $1 < q < 2$, the locus $\mathcal{B}_u$ separates the u plane into different regions, while for $0 < q < 1$, as was true for the range $q > 2$, $\mathcal{B}_u$ does not separate the u plane into different regions. In the range $q_m < q < 2$, where

$$q = q_m = \Big(\frac{5}{4}\Big)^2 = 1.5625 \ , \tag{2.2.4}$$

$\mathcal{B}_u$ crosses the real u axis vertically at three different points and separates the q plane into three regions: (i) the paramagnetic phase, which includes the infinite-temperature point $u = 1$, where $\lambda_{S,1}$ is dominant; (ii) the surrounding O phase that extends to the circle at infinity in the u plane, i.e. to the point $a = 0$,

in which phase $\lambda_{S,2}$ is dominant, and (iii) a third phase, of O type, located slightly to the left of $u = 0$, in which $\lambda_{S,2}$ is dominant. It is interesting that although $\lambda_{S,2}$ is dominant in both of the O phases, there is still a boundary that separates them completely; this is a result of the fact that on this boundary, the other λ, namely $\lambda_{S,1}$, becomes degenerate in magnitude with $\lambda_{S,2}$. Two of the points where $\mathcal{B}_u$ crosses the real axis occur where the condition (ii) holds, i.e., where the prefactor $3v + v^2 + q$ multiplying the square root in eq. (2.8), vanishes, at $v = (1/2)[-3 \pm \sqrt{9-4q}\ ]$, i.e.,

$$u = \frac{\Big[1 \pm \sqrt{9-4q}\ \Big]}{2(2-q)} \ . \tag{2.2.5}$$

For $q = 2 - \epsilon$ with $0 < \epsilon << 1$, these crossings are at $u = -1 + O(\epsilon)$ and $u \sim 1/\epsilon$. As q decreases, the smaller (larger) solution moves to the right (left). Specifically, as q decreases from 2 to 0, the larger solution decreases monotonically from infinity to 1 while the smaller one increases monotonically from -1 to $-1/2$. For example, for $q = 1.8$, the crossings in eq. (2.2.5) are at $u = (1/2)(5 \pm 3\sqrt{5}\ ) \simeq -0.854,\ 5.854$. The existence of the right crossing on the positive real u axis for $u > 1$ means that the free energy of the Potts antiferromagnet is nonanalytic at the temperature

$$T_{p,S} = \frac{J}{k_B \ln\Big[(1/2)(-1+\sqrt{9-4q}\ )\Big]} \quad \text{for} \quad 0 < q < 2 \tag{2.2.6}$$

(where both J and the log are negative). However, just as found in [13], this nonanalyticity has associated unphysical features, including negative Z, negative specific heat in the low-temperature phase, and nonexistence of a thermodynamic limit independent of boundary conditions in the low-temperature phase. As q decreases from 2 to the value q_m given above, the left and right endpoints of the line segment merge, and it shrinks to a point at $u_1 = u_2 = -4$. For this value $q = q_m$, the crossings in eq. (2.2.5) are $u = (4/7)(2 \pm \sqrt{11}\ ) \simeq 3.038,\ -0.7524$. In Fig. 6 we show $\mathcal{B}_u$ for $q = q_m$. The arc endpoints occur at $u = (20 \pm 8\sqrt{6}i\ )/49 \simeq 0.4082 \pm 0.3999i$. For $q_m < q < 2$, there is a multiple point on the negative real axis where a branch of $\mathcal{B}_u$ crosses this axis vertically and intersects with the line segment. There are also multiple points at complex-conjugate values of u where the circular arc intersects the closed curve. As q decreases from 2 to q_m, the circular arc in the left-hand complex plane enlarges while the closed curve extending into the right-hand plane shrinks and becomes convex. As q decreases below q_m, the closed curve evident to the left in Fig. 6 breaks apart, forming two complex-conjugate arcs, and in the interval $1 < q < q_m$, $\mathcal{B}_u$ no longer contains any line segment but instead consists of these complex-conjugate arcs and the closed curve to the right; an illustrative example is given in Fig. 7, where the arc endpoints occur at $u = \pm 2i$ and $u = (1/9)(4 \pm 2\sqrt{5}i\ ) \simeq 0.444 \pm 0.497i$. As q decreases toward 1, the arcs shrink to points at $u = e^{\pm i\pi/3}$. At $q = 1$, $(\mathcal{B}_u)_{qn}$ is an oval (the solution to the degeneracy equation $|u(1-u)| = 1$) that (i) crosses the real axis at $u = (1/2)(1 \pm \sqrt{5}\ )$, i.e. at approximately, 1.618 and -0.618, and (ii) crosses the imaginary axis at $u = \pm[(1/2)(-1 + \sqrt{5}\ )]^{1/2} i \simeq \pm 0.7862i$. For $0 < q < 1$, $\mathcal{B}$ consists only of two disjoint arcs, as illustrated for the value $q = 1/2$ in Fig. 8. For $q = 0$, the locus $(\mathcal{B}_u)_{qn}$ is the circular arc

$$u = \frac{1}{2} e^{i\theta} \ , \quad \frac{\pi}{2} \le \theta \le \frac{3\pi}{2} \tag{2.2.7}$$

that crosses the real axis at $u = -1/2$ and has endpoints at $u = \pm i/2$. This is qualitatively similar to $(\mathcal{B}_u)_{qn}$ for the $L_y = 2$ open strip of the square lattice at $q = 0$, which was another circular arc crossing the negative real axis at $u = -1/3$ with endpoints at $u = (-1 \pm 2\sqrt{2}i)/9$ [13].

Note that at $q = 0, 1$, one encounters the noncommutativity (1.17); if one sets q to either of these values first and then takes $n \to \infty$, the resultant $\mathcal{B}_u = \emptyset$.

Our findings for this $L_y = 2$ open strip of the triangular lattice may be contrasted with those for the $L_y = 2$ open strip of the square lattice in [13]. In the latter case, $\mathcal{B}_u$ consisted of arcs that never enclosed any regions for real $q \geq 0$.

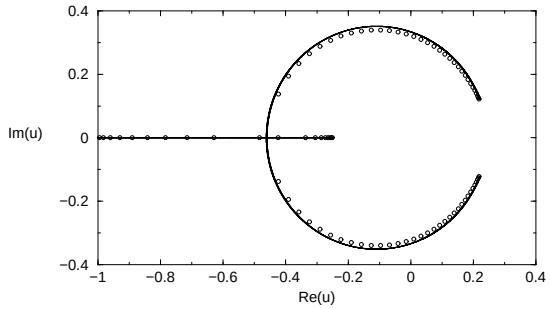

Figure 3: Locus $\mathcal{B}_u$ for the $n \to \infty$ limit of the $L_y = 2$ triangular strip, with free longitudinal boundary conditions, $\{S\}$ with $q = 10$. Zeros of $Z(S_m, q = 10, v)$ in u for $m = 20$ are shown for comparison.

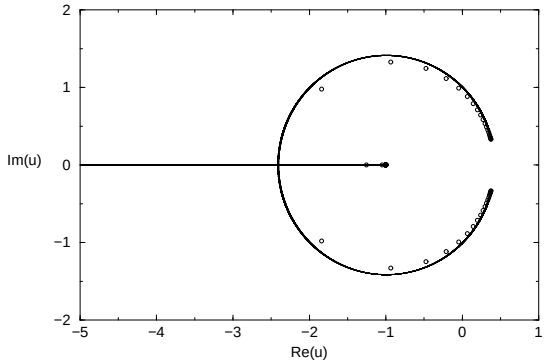

Figure 4: Locus $\mathcal{B}_u$: same as in Fig. 3 for $q = 2$.

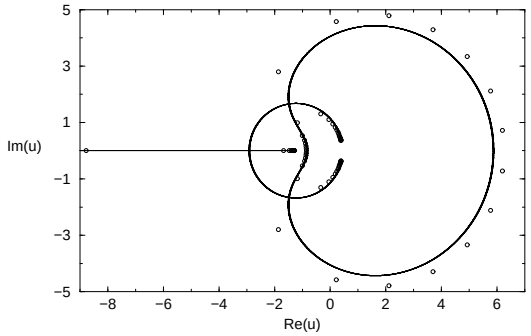

Figure 5: Locus $\mathcal{B}_u$: same as in Fig. 3 for $q = 1.8$.

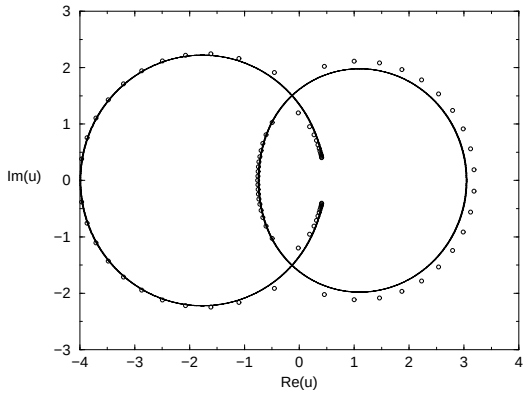

Figure 6: Locus $\mathcal{B}_u$: same as in Fig. 3 for $q = (5/4)^2$.

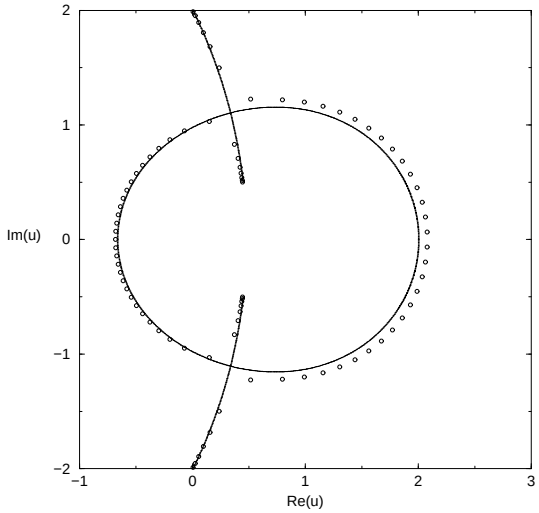

Figure 7: Locus $\mathcal{B}_u$: same as in Fig. 3 for $q = 1.25$.

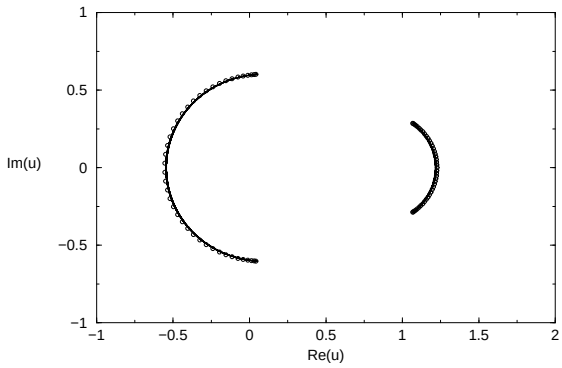

Figure 8: Locus $\mathcal{B}_u$: same as in Fig. 3 for $q = 0.5$.

3 Cyclic and Möbius Strips of the Triangular Lattice

3.1 Results for Z

By either using an iterative application of the deletion-contraction theorem for Tutte polynomials and converting the result to Z, or by using a transfer matrix method (in which one starts with a $q^2 \times q^2$ transfer matrix and generalizes to arbitrary q), one can calculate the partition function for the cyclic and Möbius ladder graphs of arbitrary length, $Z(G, q, v)$, $G = L_m,\ ML_m$. We have used both methods as checks on the calculation. Our results have the general form (1.24) with $N_\lambda = 6$:

$$Z(G_m, q, v) = \sum_{j=1}^{6} c_{G,j} (\lambda_{G,j}(q, v))^m \ , G_m = L_m, ML_m \tag{3.1.1}$$

where

$$\lambda_{L,j} = \lambda_{ML,j} \ , j = 1, ..., 6 \tag{3.1.2}$$

We find

$$\lambda_{L,1} = v^2 \tag{3.1.3}$$

and

$$\lambda_{L,5} = \lambda_{S,1} \ , \quad \lambda_{L,6} = \lambda_{S,2} \ . \tag{3.1.4}$$

The λ_j for $j = 2, 3, 4$, are the solutions of the cubic equation

$$\eta^3 - v(v^3 + 8v + 4v^2 + 2q)\eta^2 + v^2(2v^3 q + 6v^3 + 8qv + q^2 + 8v^2 + 2v^4 + 6qv^2)\eta$$

$$- \quad v^4(v+1)^2(v+q)^2 = 0 \ . \tag{3.1.5}$$

For the cyclic strip the coefficients in eq. (3.1.1) are

$$c_{L,1} = q^2 - 3q + 1 \tag{3.1.6}$$

$$c_{L,j} = q - 1 \quad \text{for} \quad j = 2, 3, 4 \tag{3.1.7}$$

$$c_{L,j} = 1 \quad \text{for} \quad j = 5, 6 \tag{3.1.8}$$

For the Möbius strip, we have

$$c_{ML,1} = -1 \tag{3.1.9}$$

and

$$c_{ML,j} = 1 \quad \text{for} \quad j = 5, 6 \ . \tag{3.1.10}$$

The coefficients $c_{ML,j}$, $j = 2, 3, 4$ are more complicated and are given by the generating function (see the appendix) by the formula given in [13].

Our exact calculations (cf. eq. (3.1.2)) yield the following general result

$$\mathcal{B}(\{L\}) = \mathcal{B}(\{ML\}) \ . \tag{3.1.11}$$

This is the same result that one of us found for the analogous strip of the square lattice [12, 13] and is in accord with the conclusion that the singular locus is the same for an infinite-length finite-width strip graph for given transverse boundary conditions, independent of the longitudinal boundary condition. Owing to the equality (3.1.11), we shall henceforth, for brevity of notation, refer to both $\mathcal{B}(\{L\})$ and $\mathcal{B}(\{ML\})$ as $\mathcal{B}(\{L\})$ and similarly for specific points on $\mathcal{B}$, such as $q_c(\{L\}) = q_c(\{ML\})$, etc.

Our main interest here is in large m and the $m \to \infty$ limit. However, for completeness, we make the following remark. If $m \ge 3$, then L_m is a (proper) graph, but the $m = 1$ and $m = 2$ cases requires special consideration; in these cases, L_m degenerates and is not a proper graph[1]. L_2 is the multigraph obtained from the complete graph K_4 [2] by doubling two non-adjacent edges (i.e., edges that do not connect to any common vertex). L_1 is the pseudograph obtained by connecting two vertices with a double edge and adding a loop to each vertex. Our calculation of $Z(L_m, q, v)$ and the corresponding Tutte polynomial $T(L_m, x, y)$ apply not just for the uniform cases $m \ge 3$ but also for the special cases $m = 1, 2$ if for $m = 2$ one includes the multiple edges and for $m = 1$ the multiple edges and loops in the evaluation of (1.1), (1.2), and (1.5). Note that in the $T = 0$ case for the antiferromagnet, the resulting partition function, or equivalently, the chromatic polynomial, is not sensitive to multiple edges, i.e. is the same for a graph in which two vertices are connected by one edge or multiple edges; however, the general partition function (Tutte polynomial) is sensitive to multiple edges. The chromatic polynomial is sensitive to loops and vanishes identically when a pseudograph has any loops.

3.2 Special values and expansions of λ's

We discuss some special cases. First, for the zero-temperature Potts antiferromagnet, i.e. the case $a = 0$ ($v = -1$), the partition functions $Z(L_m, q, v)$ and $Z(ML_m, q, v)$ reduce, in accordance with the general result (1.6), to the respective chromatic polynomials $P(L_m, q)$ and $P(ML_m, q)$ [32] with λ_j's comprised of the four terms 1, $(q-2)^2$, and $(1/2)[5 - 2q \pm \sqrt{9-4q}]$. The two remaining $\lambda_{L,j}$'s vanish in this limit. (Since only four $\lambda_{L,j}$'s occur in the chromatic polynomial, a different numbering convention was used in [32] than here, where, in general, six occur.) For the infinite-temperature value $a = 1$, we have $\lambda_{L,j} = 0$ for $j = 1, 2, 3, 4, 6$, while $\lambda_{L,5} = q^2$, so that $Z(G, q, a = 1) = q^{2m} = q^n$ for $G = L_m, \ ML_m$, in accord with the general result (1.10). For the real interval $q \ge 3$ and the region R_1 to which one can analytically continue from this interval (see Fig. 9 below), $W = q - 2$. Hence, $W = 1$ at $q = 3$. A technical remark is the following: one can, and it is convenient to, take the $n \to \infty$ limit with $m = 0$ mod 3, so that, by eqs. (1.13) and (1.16), $P = 3!$, so

[1] A proper graph has no multiple edges or loops, where a loop is an edge that connects a vertex to itself. A multigraph may contain multiple edges, but no loops, while a pseudograph may contain both multiple edges and loops [9, 11].

[2] The complete graph K_p is the graph with p vertices each of which is adjacent to all of the other vertices.

that the limit for W exists at $a = 0$ as well as at $a \neq 0$. In contrast, if one took $n \to \infty$ using all positive integer values of m, then, strictly speaking, the limit for W in eq. (1.7) would not exist for $a = 0$, since P would have the nonconvergent values $6, 0, 0, 6, , ..$ for $m = 3k, 3k+1, 3k+2, 3k+3, ..$ For the Möbius longitudinal boundary condition, no such convenient choice is possible, since $\chi = 4$ for all m; here there is a noncommutativity: if one starts with q slightly larger than 3, takes $n \to \infty$ to calculate W, and then lets $q \searrow 3$, one gets $W(q = 3) = 1$, but if one sets $q = 3$ first and then lets $n \to \infty$, one gets $W(q = 3) = 0$.

At $q = 0$ (with appropriate choices of branch cuts) we find that

$$\lambda_{L,1} = \lambda_{L,3} = v^2 \tag{3.2.1}$$

$$\lambda_{L,2} = \lambda_{L,5} = \frac{v^2}{2}\Big[v^2 + 4v + 7 + (v+3)\sqrt{v^2+2v+5}\,\Big] \tag{3.2.2}$$

and

$$\lambda_{L,4} = \lambda_{L,6} = \frac{v^2}{2}\Big[v^2 + 4v + 7 - (v+3)\sqrt{v^2+2v+5}\,\Big]\ . \tag{3.2.3}$$

Since there are dominant terms that are degenerate, namely $\lambda_{L,2} = \lambda_{L,5}$, it follows that

$$q = 0 \quad \text{is on} \quad \mathcal{B}_q(\{L\}) \quad \forall\ a\ . \tag{3.2.4}$$

This was also true of the circuit graph and cyclic and Möbius square strips with $L_y = 2$ for which the general Potts model partition function (Tutte polynomial) was calculated in [13]. For $q = 0$, the coefficients $c_j = 1$ for $j = 1, 5, 6$ and $c_j = -1$ for $j = 2, 3, 4$ so that the equal terms cancel each other pairwise, yielding $Z(L_m, q = 0, v) = 0$, in accordance with the general result (1.8). The noncommutativity (1.17) occurs here: $\exp(f_{nq}) = 0$, while $|\exp(f_{qn})| = |\lambda_{L,5}|^{1/2}$.

At $q = 1, 2$ we again encounter noncommutativity in the calculation of the free energy. For $q = 1$, $f_{nq} = 2\ln a = 2K$, while f_{qn} depends on which phase one is in for a given value of a. For $0 < a < a_c(q = 1)$, where, from eq. (3.3.4), $a_c(q = 1) = (1/2)(-1 + \sqrt{5}) \simeq 0.6180$, $f_{qn} = (1/2)\ln\lambda_{L,c}$, where $\lambda_{L,c}$ is the cube root that is dominant in this phase (corresponding to $(1/2)[5 - 2q + \sqrt{9-4q}]$ for $a \to 0$), while for $a > a_c(q = 1)$, $f_{qn} = (1/2)\ln\lambda_{L,5}$.

Similarly, for $q = 2$, again with an appropriate choice of branch cuts,

$$\lambda_{L,1} = \lambda_{L,3} = v^2 \tag{3.2.5}$$

$$\lambda_{L,(2,4)} = \frac{v(v+1)}{2}\left[v^2 + 3v + 4 \pm \Big[v(v+1)(v^2+5v+8)\Big]^{1/2}\right] \tag{3.2.6}$$

and

$$\lambda_{L,(5,6)} = \frac{(v+1)(v+2)}{2}\left[(v^2+v+2) \pm \Big[(v+1)(v+2)(v^2-v+2)\Big]^{1/2}\right]\ . \tag{3.2.7}$$

For this value, $q = 2$, the coefficients are $c_{L,1} = -1$, while $c_{L,j} = 1$, $2 \le j \le 6$; hence, the $(\lambda_{L,1})^m$ and $(\lambda_{L,3})^m$ terms cancel each other and make no contribution to Z, which reduces to

$$Z(L_m, q = 2, v) = \sum_{j=2,4,5,6} (\lambda_{L,j})^m \tag{3.2.8}$$

Hence also, $f_{qn} \neq f_{nq}$ at $q = 2$.

We observe that the λ_j's have a more symmetric form for $q = 2$ when expressed in terms of the variable u:

$$\lambda_{L,1,u} = \lambda_{L,3,u} = u^2(1-u)^2 \tag{3.2.9}$$

$$\lambda_{L,(2,4),u} = \frac{(1-u)}{2}\Big[1+u+2u^2 \pm \Big[(1-u)(1+3u+4u^2)\Big]^{1/2}\Big] \tag{3.2.10}$$

and

$$\lambda_{L,(5,6),u} = \frac{(1+u)}{2}\Big[1-u+2u^2 \pm \Big[(1+u)(1-3u+4u^2)\Big]^{1/2}\Big] \ . \tag{3.2.11}$$

One sees that each member of the pair $\lambda_{L,(2,4),u}$ is equal to the respective member of the pair $\lambda_{L,(5,6),u}$ with the replacement $u \to -u$. It follows that $|\lambda_{L,2,u}| = |\lambda_{L,5,u}|$ and $|\lambda_{L,4,u}| = |\lambda_{L,6,u}|$ for u pure imaginary.

In general, for $q \in \mathbb{Z}_+$, the partition function $Z(L_m, q, v)$ for the cyclic width $L_y = 2$ strip of the triangular lattice is identical to the partition function for the 1D q-state Potts model with nearest-neighbor and next-nearest-neighbor spin-spin couplings that are equal in magnitude. This equality can be seen easily by redrawing the strip of the triangular lattice as a line with additional couplings between next-nearest-neighbor vertices on this line. In Ref. [42] Tsai and one of us calculated Z for the latter model (with, in general, unequal nearest and next-nearest-neighbor spin-spin couplings). Hence, in particular, the $q = 2$ and $q = 3$ of eq. (3.1.1) coincide with the results in (section IX of) [42].

In order to study the zero-temperature critical point in the ferromagnetic case and also the properties of the complex-temperature phase diagram, we calculate the $\lambda_{G,j,u}$'s corresponding to the $\lambda_{G,j}$'s, using eq. (1.27). In the vicinity of the point $u = 0$ we have

$$\lambda_{L,1,u} = u^2(1-u)^2 \tag{3.2.12}$$

and the Taylor series expansions

$$\lambda_{L,2,u} = 1 - 2u^3 + 2(q-1)u^4 + O(u^5) \tag{3.2.13}$$

$$\lambda_{L,3,u} = u^2 + O(u^3) \tag{3.2.14}$$

$$\lambda_{L,4,u} = u^2 + O(u^3) \tag{3.2.15}$$

$$\lambda_{L,5,u} = 1 + 2(q-1)u^3\Big[1+u+O(u^2)\Big] \tag{3.2.16}$$

$$\lambda_{L,6,u} = u^2 + 2(q-2)u^3 + O(u^4) \ . \tag{3.2.17}$$

Hence, at $u = 0$, $\lambda_{L,2,u}$ and $\lambda_{L,5,u}$ are dominant and $|\lambda_{L,2,u}| = |\lambda_{L,5,u}|$, so that the point $u = 0$ is on $\mathcal{B}_u$ for any $q \neq 0, 1$, where the noncommutativity (1.17) occurs. To determine the angles at which the branches of $\mathcal{B}_u$ cross each other at $u = 0$, we write u in polar coordinates as $u = re^{i\theta}$, expand the degeneracy equation $|\lambda_{L,2,u}| = |\lambda_{L,5,u}|$, for small r, and obtain $qr^3\cos(3\theta) = 0$, which implies that (for $q \neq 0, 1$) in the limit as $r = |u| \to 0$,

$$\theta = \frac{(2j+1)\pi}{6} \ , \quad j = 0, 1, ..., 5 \tag{3.2.18}$$

or equivalently, $\theta = \pm\pi/6$, $\pm\pi/2$, and $\theta = \pm 5\pi/6$. Hence there are six curves forming three branches of $\mathcal{B}_u$ intersecting at $u = 0$ and successive branches cross at an angle of $\pi/3$. The point $u = 0$ is thus a multiple point on the algebraic curve $\mathcal{B}_u$, in the technical terminology of algebraic geometry (i.e., a point where several branches of an algebraic curve cross [43]). In the vicinity of the origin, $u = 0$, these branches define six complex-temperature phases: the paramagnetic (PM) phase for $-\pi/6 \le \theta \le \pi/6$, together with the phases O_j for $1 \le j \le 5$, with O_j occupying the sector $(2j-1)\pi/6 \le \theta \le (2j+1)\pi/6$. Note that $O_3 = O_3^*$, $O_4 = O_2^*$, and $O_5 = O_1^*$. For the case of interest here, namely, $q > 0$, $\lambda_{L,5,u}$ is dominant in the PM phase and in the O_2 and O_2^* phases, while $\lambda_{L,2,u}$ is dominant in the O_1, O_1^*, and O_3 phases.

One of our interesting findings is that for $q = 2$ and for $q = 3$ the Potts antiferromagnet on the infinite-length, width $L_y = 2$ strip of the triangular lattice has a zero-temperature critical point. (As must be the case for this to be physical, this is independent of the longitudinal boundary conditions.) In the $q = 2$ Ising case, this involves frustration, and the 2D Ising antiferromagnet on the triangular lattice also has a $T = 0$ critical point [44]. In contrast, for the $q = 3$ case, the $T = 0$ critical point does not involve any frustration, and the q value at which this occurs for our $L_y = 2$ strip is different than the value, $q = 4$, where the Potts antiferromagnet has a $T = 0$ critical point on the full 2D triangular lattice. In order to study the $T = 0$ critical point for the $L_y = 2$ strip for these two values of q, it is useful to calculate expansions of the λ_j's; only $\lambda_{L,5}$ and $\lambda_{L,2}$ are necessary for physical thermodynamic properties, while the full set of $\lambda_{L,j}$, $j = 1, 2, .., 6$ is necessary for the study of the singular locus $\mathcal{B}$.

For $q = 2$, besides the exact expressions $\lambda_{L,1} = \lambda_{L,3} = (1-a)^2$ from eq. (3.2.5), we have the expansions

$$\lambda_{L,(2,4)} = -a + \frac{a^2}{2}(1+a^2) \pm i\sqrt{a}\Big[-a + \frac{9}{8}a^2 + O(a^3)\Big] \tag{3.2.19}$$

and

$$\lambda_{L,(5,6)} = a + \frac{a^2}{2}(1+a^2) \pm \sqrt{a}\Big[a + \frac{9}{8}a^2 + O(a^3)\Big] \ . \tag{3.2.20}$$

Note that (i) these are not Taylor series expansions in a, but rather in the variable $\sqrt{a}$, and (ii) each member of the pair $\lambda_{L,(2,4)}$ is equal to the respective member of the pair $\lambda_{L,(5,6)}$ with the replacement $a \to -a$. As shown above, for f_{nq} and $\mathcal{B}_{nq}$, where one sets $q = 2$ first and then takes $n \to \infty$, $\lambda_{L,j}$, $j = 1, 3$, make no contribution, and $\mathcal{B}_{nq}$ is determined by the degeneracy in magnitude of $\lambda_{L,j}$, $j = 2, 4, 5, 6$. From the expansions (3.2.19) and (3.2.20), it follows that in the neighborhood of the point $a = 0$, $(\mathcal{B}_a)_{nq}$ is determined by the equation $|\lambda_{L,2}| = |\lambda_{L,5}|$ and is a vertical line segment along the imaginary a axis. This will be discussed further below (see Fig. 16).

For $q = 3$, besides the exact expression $\lambda_{L,1} = (1-a)^2$, we calculate the expansions

$$\lambda_{L,(2,3)} = e^{\pm 2\pi i/3} - 2e^{\pm \pi i/3}a + \Big(-1 \pm \frac{2i\sqrt{3}}{3}\Big)a^2 + O(a^3) \tag{3.2.21}$$

(where the upper (lower) sign applies for $j = 2$ ($j = 3$));

$$\lambda_{L,4} = 4a^2 - 4a^3 + O(a^4) \tag{3.2.22}$$

$$\lambda_{L,5} = 1 + 6a - 3a^2 + O(a^3) \tag{3.2.23}$$

and

$$\lambda_{L,6} = 4a^2 - 28a^3 + O(a^4) \ . \tag{3.2.24}$$

There are thus four dominant $\lambda_{L,j}$'s at $a = 0$, viz., those with $j = 1, 2, 3, 5$, which satisfy $|\lambda_{L,j}| = 1$. Writing $a = \rho e^{i\phi}$ and expanding the dominant $\lambda_{L,j}$'s in the neighborhood of $a = 0$, we obtain

$$|\lambda_{L,1}|^2 = 1 - 4\rho\cos\phi + O(\rho^2) \tag{3.2.25}$$

$$|\lambda_{L,(2,3)}|^2 = 1 - 4\rho\cos(\phi \mp \pi/3) + O(\rho^2) \tag{3.2.26}$$

and

$$|\lambda_{L,5}|^2 = 1 + 12\rho\cos\phi + O(\rho^2) \ . \tag{3.2.27}$$

Equating dominant $|\lambda_{L,j}|$'s, it follows that in the neighborhood of $a = 0$, $\mathcal{B}_a$ consists of four curves, forming complex-conjugate pairs, passing through $a = 0$ at the angles

$$\phi = \pm arctan\Big(\frac{7\sqrt{3}}{3}\Big) \simeq 76.10^\circ \ . \tag{3.2.28}$$

and

$$\phi = \pm\frac{5\pi}{6} = \pm 150^\circ \tag{3.2.29}$$

In Fig. 18 below we show $\mathcal{B}_a$ for this case.

3.3 $\mathcal{B}_q(\{L\})$ for fixed a

3.3.1 Antiferromagnetic case $0 \le a \le 1$

We begin with the case $a = 0$, i.e. the $T = 0$ limit of the Potts antiferromagnet. The locus $\mathcal{B}_q$ for this case was stated in [31] and given as Fig. 3 in [32]. This locus $\mathcal{B}_q$, shown as Fig. 9 here, separates the complex q plane into three different regions: (i) R_1, including the segments $q > 3$ and $q < 0$ on the real axis, where $W = (q-2)$; (ii) R_2, including the real interval $2 < q < 3$, in which $|W| = 1$; and (iii) R_3, including the real segment $0 < q < 2$, in which $|W| = [(1/2)(5 - 2q + \sqrt{9-4q}\ )]^{1/2}$. At $q = q_c$ there are actually four terms that are degenerate in magnitude,

$$\lambda_{L,1} = \lambda_{L,5} = |\lambda_{L,2}| = |\lambda_{L,3}| = 1 \quad \text{at} \quad q = 3 \quad \text{for} \quad a = 0 \tag{3.3.1}$$

corresponding to the property that this is a multiple point on $\mathcal{B}_q$ (in the terminology of algebraic geometry) where four curves intersect. In contrast, the other two points at which $\mathcal{B}_q$ crosses the real axis, at $q = 0$ and $q = 2$, involve only the minimal number (two) of degenerate magnitudes and are hence not multiple points. Evidently, $q_c(\{L\}) = 3$ for this $a = 0$ case.

We show calculations of $\mathcal{B}_q(\{L\})$ in Figs. 10, 11, and 12 for finite temperature. As a increases from 0, rather than having a fourfold degeneracy of λ's at $q = 3$, as in the $a = 0$ case, eq. (3.3.1), one only has a twofold degeneracy,

$$|\lambda_{L,5}| = |\lambda_{L,1}| \tag{3.3.2}$$

This occurs at the point

$$q_c(\{L\}) = q_c(\{ML\}) = \frac{(1-a)(3+2a)}{1+a} = -\frac{v(2v+5)}{v+2} \ . \tag{3.3.3}$$

Corresponding to this value of q is the pair

$$a_c(\{L\})_\pm = a_c(\{ML\})_\pm = \frac{1}{4}\Big[-(q+1) \pm \sqrt{q^2-6q+25}\ \Big] \ . \tag{3.3.4}$$

As a increases from 0 to 1, $q_c(\{L\})$ decreases monotonically from 3 to 0. Over the interval $0 < a < a_d$, where

$$a_d = \frac{1}{4}(-3 + \sqrt{17}\ ) = 0.280776.. \tag{3.3.5}$$

the innermost region, R_2 continues to exist, but shrinks in size. Its left-hand boundary on the real q axis, where it is contiguous with region R_3, continues to lie at

$$q_{R_2-R_3} = 2 \quad \text{for} \quad 0 < a < a_d \ . \tag{3.3.6}$$

This follows from the fact that this point is the real solution to the degeneracy equation of leading terms $|\lambda_{L,1}| = |\lambda_{L,3}|$, and these are both equal (to v^2) at $q = 2$. As a increases through the value $a = a_d$, $q_c(\{L\})_{a=a_d} = 2$, so this innermost region R_2 disappears; this can be seen from the fact that its right-hand boundary point q_c becomes equal to its left-hand boundary point, given by $q_{R_2-R_3}$. Thus, for $a_d < a < 1$, the locus $\mathcal{B}_q$ separates the q plane into only two regions, R_1 and R_3.

The Potts antiferromagnet has a phase transition at the temperature given by the upper choice of the sign in eq. (3.3.4), i.e.,

$$T_{p,L} = \frac{J}{k_B \ln(a_c(\{L\})_+)} , \qquad 0 < q < 3 \tag{3.3.7}$$

(where both J and the log are negative). However, just as was found for the analogous phase transition of the Potts model on the infinite-length $L_y = 2$ strip of the square lattice (which occurred for the range $0 < q < 2$ except for f_{nq} for the integral value $q = 1$) [13], the present phase transition involves unphysical properties, including negative Z, negative specific heat in the low-temperature phase, and non-existence of a thermodynamic limit independent of boundary conditions in the low-temperature phase. The general existence of such pathologies was noted in [41]. As a increases further to 1, $\mathcal{B}_q$ contracts in to a point at the origin, $q = 0$.

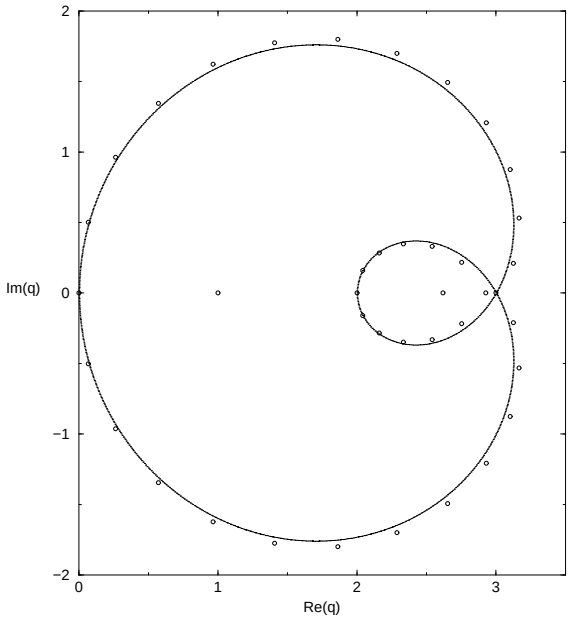

Figure 9: Locus $\mathcal{B}_q(\{L\})$ for the $n \to \infty$ limit of the $L_y = 2$ cyclic or Möbius triangular strip for $a = 0$, i.e., the $T = 0$ limit of the Potts antiferromagnet. Chromatic zeros for $m = 20$ (so that Z is a polynomial of degree $n = 40$ in q) are shown for comparison.

3.3.2 Ferromagnetic range $a \geq 1$

For the Potts ferromagnet, as T decreases from infinity, i.e. a increases above 1, the locus $\mathcal{B}_q$ forms a lima-bean shaped curve shown for a typical value, $a = 2$, in Fig. 13. Besides the generally present crossing at $q = 0$, the point $q_c(\{L\})$ at which $\mathcal{B}_q$ crosses the real q axis now occurs at negative q values. As was true

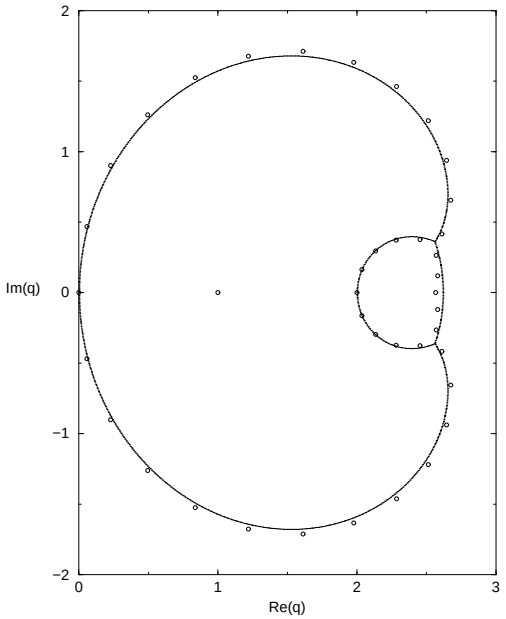

Figure 10: Locus $\mathcal{B}_q(\{L\})$: same as Fig. 9 for $a = 0.1$ (finite-temperature Potts antiferromagnet).

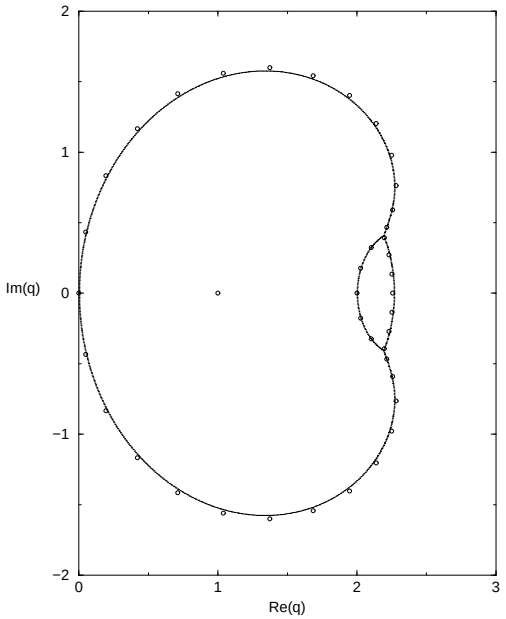

Figure 11: Locus $\mathcal{B}_q(\{L\})$: same as Fig. 9 for $a = 0.2$.

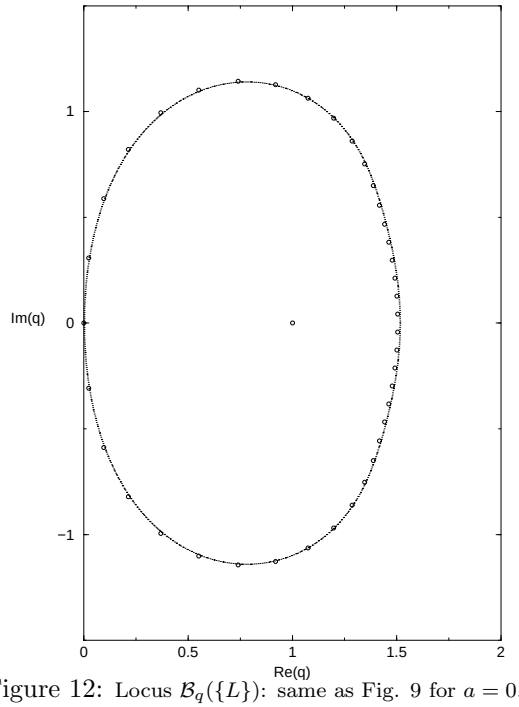

Figure 12: Locus $\mathcal{B}_q(\{L\})$: same as Fig. 9 for $a = 0.5$.

of the model on the analogous width $L_y = 2$ cyclic and Möbius strips of the square lattice [13], for physical temperatures, the locus $\mathcal{B}_q$ for the Potts ferromagnet does not cross the positive real q axis. Note that this locus does have some support in the $Re(q) > 0$ half plane, away from the real axis, which was also true of the analogous locus for the $L_y = 2$ cyclic and Möbius square strip.

3.4 $\mathcal{B}_u(\{L\})$ for Fixed q

We next proceed to the slices of $\mathcal{B}$ in the plane defined by the temperature Boltzmann variable u, for given values of q, starting with large q. In the limit $q \to \infty$, the locus $\mathcal{B}_u(\{L\})$ is reduced to $\emptyset$. This follows because for large q, there is only a single dominant λ_j, namely

$$\lambda_{L,5} \sim q^2 + 4qv + O(1) \quad \text{as} \quad q \to \infty \ . \tag{3.4.1}$$

Note that in this case, one gets the same result whether one takes $q \to \infty$ first and then $n = 2m \to \infty$, or $n \to \infty$ and then $q \to \infty$, so that these limits commute as regards the determination of $\mathcal{B}_u$.

We first consider values of $q \neq 0, 1, 2$, so that no noncommutativity occurs, and $(\mathcal{B}_u)_{nq} = (\mathcal{B}_u)_{qn} \equiv \mathcal{B}_u$. As discussed above, it is convenient to use the u plane since $\mathcal{B}_u$ is compact in this plane, except for the cases $q = 2$ and $q = 3$, whereas $\mathcal{B}_u$ is noncompact because of the antiferromagnetic zero-temperature critical point at $a = 1/u = 0$.

Extending the discussion in [13] to the case of the strip of the triangular lattice, we observe that the property that the singular locus $\mathcal{B}_u$ passes through the $T = 0$ point $u = 0$ for the Potts model with periodic boundary but not with free boundary conditions means that the use of periodic boundary conditions yields a singular locus that manifestly incorporates the zero-temperature critical point, while this is not manifest in $\mathcal{B}_u$ when calculated using free boundary conditions.

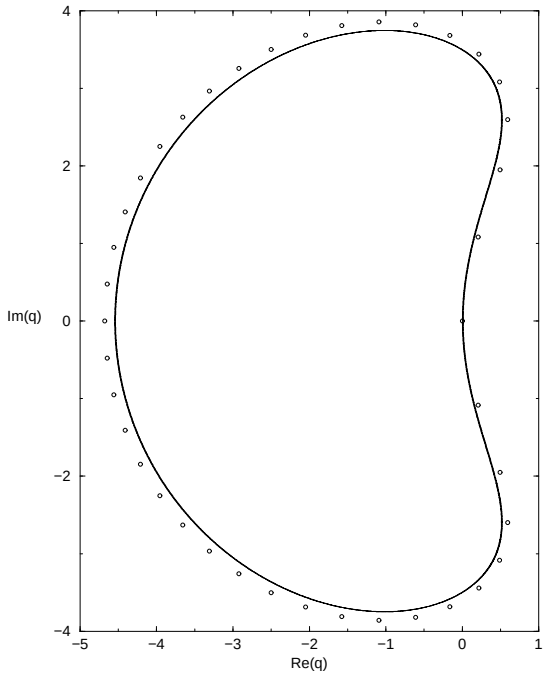

Figure 13: Locus $\mathcal{B}_q$ for the $n \to \infty$ limit of the cyclic or Möbius triangular strip, $\{L\}$ or $\{ML\}$, with $a = 2$ (finite-temperature Potts ferromagnet).

For $q = 10$, the locus $\mathcal{B}_u$ is shown in Fig. 14. Six curves on $\mathcal{B}_u$ run into the origin, $u = 0$, at the angles given in general in eq. (3.2.18). The six corresponding complex-temperature phases contiguous to the origin, $u = 0$ exhaust the totality of such phases; i.e., there are no such phases that are disjoint from $u = 0$. The $\lambda_{L,j}$'s that are dominant in these phases were given above, after eq. (3.2.18). As is evident in Fig. 14, part of $\mathcal{B}_u$ forms a approximately circular curve. The locus $\mathcal{B}_u$ also includes a line segment on the negative real u axis along which $\lambda_{L,5}$ and $\lambda_{L,6}$ are dominant and are equal in magnitude as complex conjugates of each other.

For $q = 2$, the locus $(\mathcal{B}_u)_{nq}$ is shown in Fig. 15. One sees that, in addition to the six curves intersecting at the ferromagnetic zero-temperature critical point $u = 0$, $\mathcal{B}_u$ has multiple points at $u = \pm i$ where four curves intersect. The complex-temperature phases in the vicinity of $u = 0$ were determined above after eq. (3.2.18), and these exhaust all complex-temperature phases, i.e. there is none that does not extend in to $u = 0$.

For $q = 3$, the locus $\mathcal{B}_u$ was given as Fig. 10 in Ref. [42] and is shown with associated partition function zeros in Fig. 17. In this case, in addition to the six phases that are contiguous at $u = 0$, there is evidently another O phase that includes the negative real axis for $u < -1$, and a complex conjugate pair of O phases extending outward from the intersection points at $u = e^{\pm 2\pi i/3}$ toward the upper and lower left. At these intersection (multiple) points, six curves on $\mathcal{B}_u$ intersect, just as was true at $u = 0$. The existence of the intersection points on $\mathcal{B}_u$ at $u = e^{\pm 2\pi i/3}$ for the strip would suggest that such points could also be present on the locus $\mathcal{B}_u$ for the $q = 3$ Potts model on the full triangular lattice. Since this model has not been exactly solved, one can only try to infer $\mathcal{B}_u$ from complex-temperature (Fisher) zeros of the partition function calculated for large triangular lattices [45, 50, 51]. These are consistent with this possibility (see,

e.g., Fig. 1 of [45] or Figs. 5-7 of [51]) although the zeros show such a high degree of scatter in the $Re(a) < 0$ half-plane that one cannot draw a very decisive conclusion from them.

For $q = 4$ we show the locus $\mathcal{B}_u$ in Fig. 19. In this case, we remark, in

For the study of the zero-temperature critical point of the Potts antiferromagnet on the $L_y = 2$ cyclic and Möbius strips of the triangular lattice, it is useful to display the singular locus $\mathcal{B}_a$ in the a plane, since the critical point occurs at $a = 0$. We show these plots for $q = 2$ and 3 in Figs. 16 and 18. For $q = 2$, the boundary $\mathcal{B}_a$ has a multiple point at $a = \pm i$ where four branches intersect. For $q = 3$, four curves on $\mathcal{B}_a$ pass through $a = 0$ at the angles given in eqs. (3.2.28) and (3.2.29). Note that that the curves that leave the origin at the angles ϕ given in eq. (3.2.28) rapidly bend toward the vertical and then back toward the left, so that the complex-temperature phase that is contiguous with $u = 0$ and lies in the angular wedges between 76° and 150°, and its complex-conjugate, are rather narrow. The multiple points at $a = e^{\pm 2\pi i/3}$ have been described above.

In Figs. 21 and 20 we show the analogous loci $\mathcal{B}_u$ for the $L_y = 2$ cyclic or Möbius strip of the square lattice studied in [13] for comparison. A particularly striking difference is that, since the $q = 3$ Potts antiferromagnet is (is not) critical on the $L_y = 2$ strip of the triangular (square) lattice, the resultant locus $\mathcal{B}_u$ passes through (does not pass through) $1/u = a = 0$, respectively. The Ising model, $q = 2$ has both ferromagnetic and antiferromagnetic $T = 0$ critical points on both the $L_y = 2$ square and triangular lattice strips, and hence for both strips, $\mathcal{B}_u$ passes through $1/u = a = 0$.

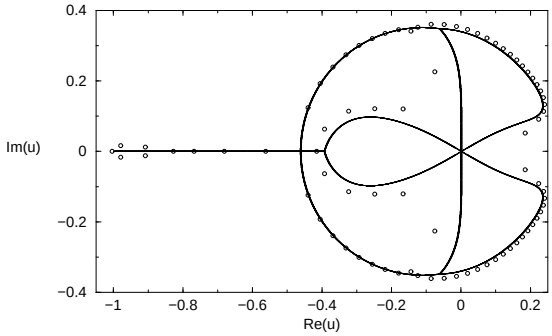

Figure 14: Locus $\mathcal{B}_u(\{L\})$ for the $n \to \infty$ limit of the cyclic or Möbius triangular strip, $\{L\}$ or $\{ML\}$, with $q = 10$. Partition function zeros are shown for $m = 20$, so that Z is a polynomial of degree $e = 4m = 80$ in v and hence, up to an overall factor, in u).

3.5 Connections Between $\mathcal{B}$ for Strips and 2D Lattices

In earlier work [53, 54, 13], it was shown that although the physical thermodynamic properties of a discrete spin model are, in general, different in 1D or infinite-length, finite-width strips, which are quasi-1D systems, and in higher dimensions, nevertheless, exact solutions for $\mathcal{B}_u$ in 1D and quasi-1D systems can give insight into $\mathcal{B}_u$ in 2D. This was shown, in particular, for the $q = 2$ Ising special case of the Potts model, where the comparison can be made rigorously since the model is exactly solvable in 2D. It will often be convenient below to use the equivalent locus in the $a = 1/u$ plane, $\mathcal{B}_a$. In [24, 26, 25, 12, 32] it was also noted how exact calculations of $\mathcal{B}_q$ and W on infinite-length, finite-width strips can give information about the behavior of these quantities on 2D lattices.

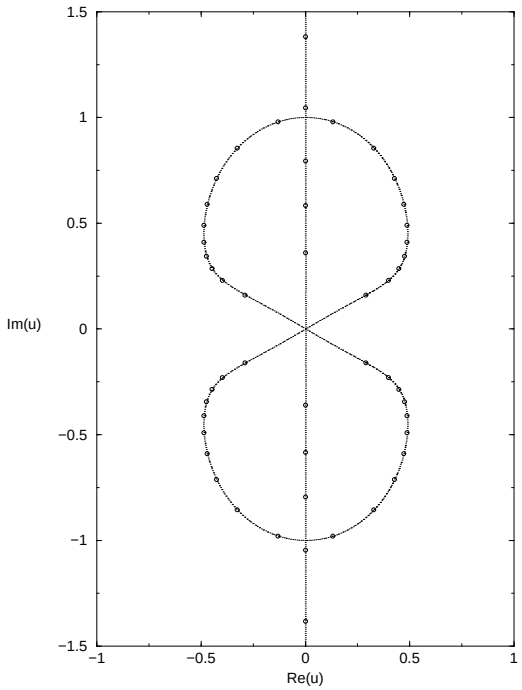

Figure 15: Locus $\mathcal{B}_u(\{L\})$: same as Fig. 14 for $q = 2$.

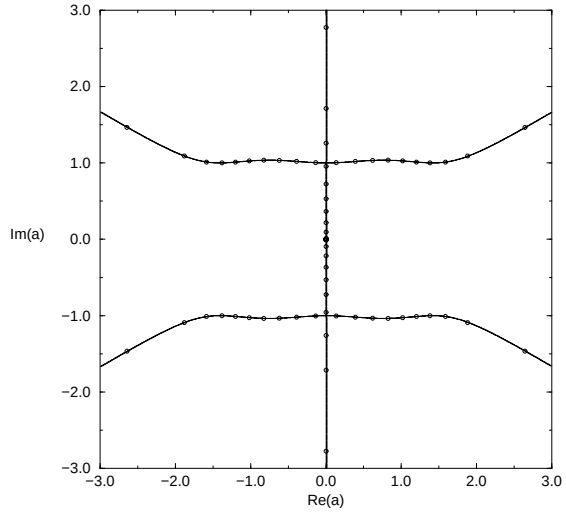

Figure 16: Locus $\mathcal{B}_a$ for the $n \to \infty$ limit of the cyclic or Möbius triangular strip, $\{L\}$ or $\{ML\}$, with $q = 2$.

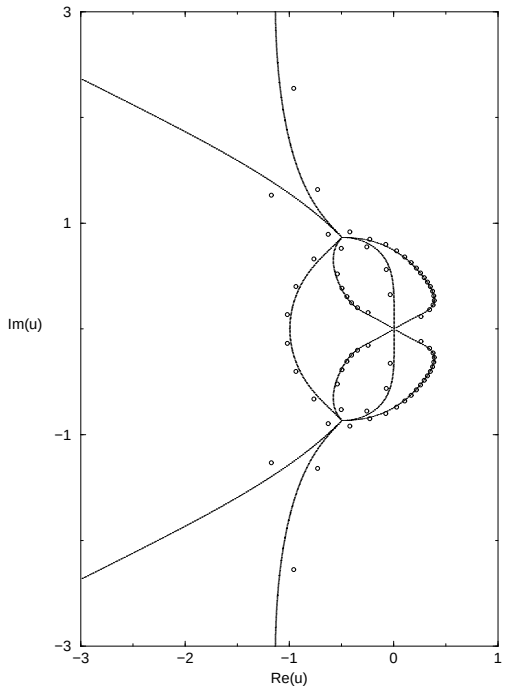

Figure 17: Locus $\mathcal{B}_u(\{L\})$: same as Fig. 14 for $q = 3$.

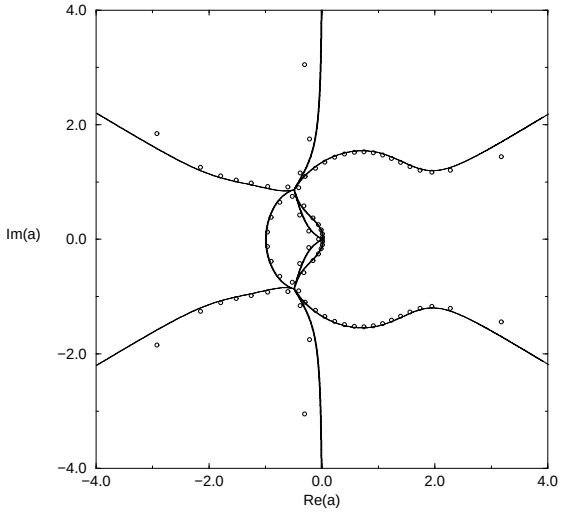

Figure 18: Same as Fig. 16 for $q = 3$.

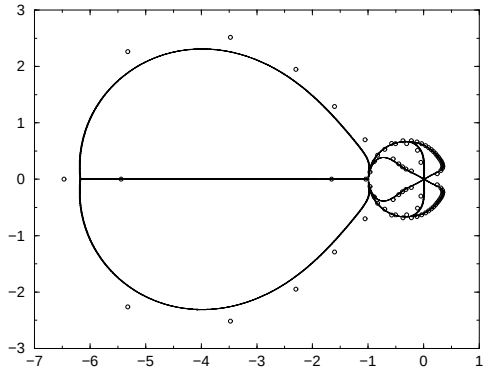

Figure 19: Same as Fig. 15 for $q = 4$.

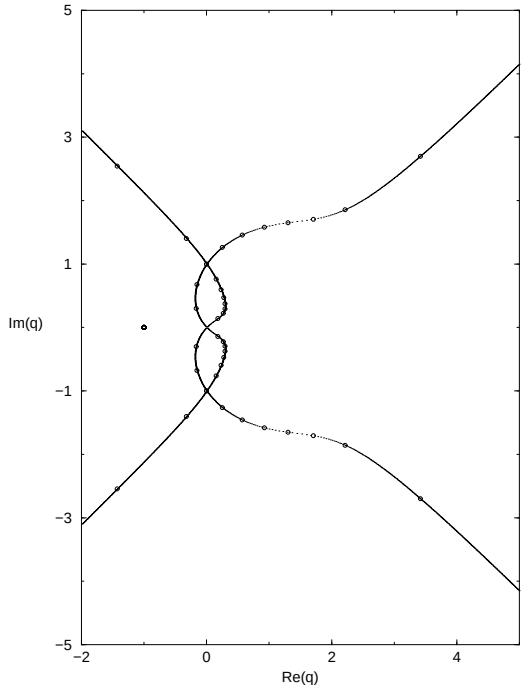

Figure 20: Locus $\mathcal{B}_u = \mathcal{B}_a$ for the $L_y = 2$ square strip with $q = 2$. Partition function zeros are shown for $m = 20$ ($e = 60$).

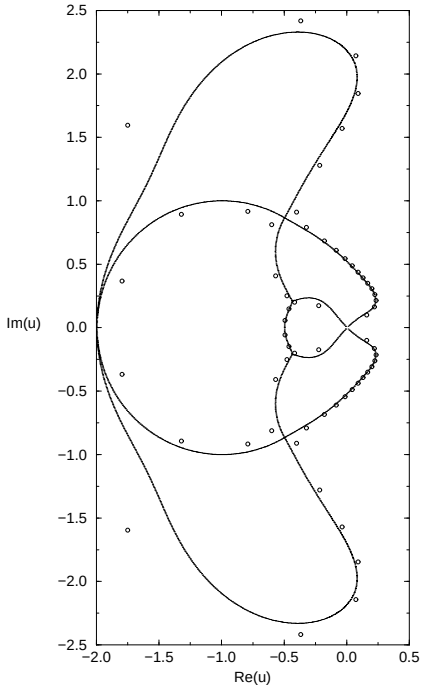

Figure 21: Locus $\mathcal{B}_u$ for the $L_y = 2$ square strip with $q = 3$. Partition function zeros are shown for $m = 20$ (so that Z is a polynomial of degree $e = 3m = 60$ in v and hence, up to an overall factor, in u).

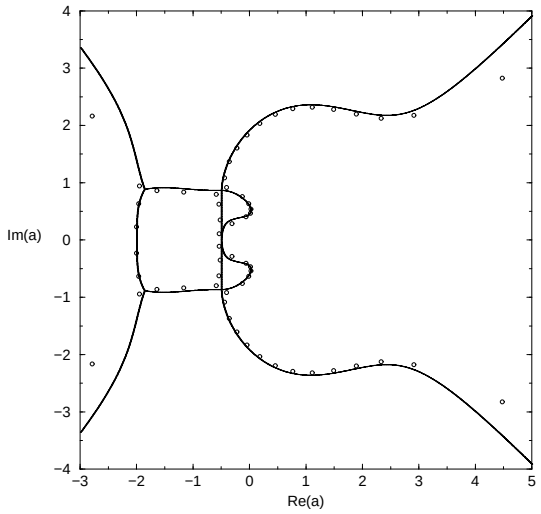

Figure 22: Locus $\mathcal{B}_a$ for the $L_y = 2$ square strip with $q = 3$. Partition function zeros are shown for $m = 20$ (so that Z is a polynomial of degree $e = 3m = 60$ in v and hence a).

In Ref. [13], the connection between $\mathcal{B}_a$ on strips and in on the full 2D square lattice was studied; here we shall do this for the triangular lattice. Again, it is natural to start with the $q = 2$ Ising case, where one has exact results both for the strip and the full triangular lattice. The comparisons made in [13] and here enable one to formulate a reasonably systematic procedure for making transformations on an exactly calculated locus $\mathcal{B}_a$ for the Potts model on an infinite-length, finite-width strip of a given lattice, in order to construct at least a qualitatively correct locus $\mathcal{B}_a$ on the corresponding 2D lattice. As emphasized in [13], this represents a new and powerful way of obtaining information about complex-temperature phase diagrams of spin models in 2D (indeed perhaps also higher dimensions) from exact results on strips. It will be recalled that the conventional approach has been the rather laborious procedure of performing exact calculations of the partition function on finite 2D lattices of various sizes with various boundary conditions [45]-[49]. Although some features of $\mathcal{B}_a$ for the Potts model, such as the circle $|a-1| = \sqrt{q}$ for $Re(a) > 0$ are evident with this conventional procedure, the comlex-temperature (Fisher) zeros often exhibit such considerable scatter for $Re(a) < 0$ that it is difficult to infer the structure of the locus $\mathcal{B}_a$ in this region. One method was to combine calculations of the zeros with dlog Padé and differential approximant analyses of low-temperature series expansions so as to localize accurately certain points on the complex-temperature boundary [49]-[51]. This method was motivated by the fact that complex-temperature singularities in such quantities as specific heat and magnetization for the 2D Ising model can be calculated exactly and they occur at known points on the complex-temperature boundaries for respective 2D lattices; it was also shown that this was true for the susceptibility, where no exact calculation exists [39, 52]. However, while this method avoids the problem of the scatter in Fisher zeros, it only localizes certain points on $\mathcal{B}_a$. The present method is complementary in that it enables one to gain, at least qualitatively, an idea of the global structure of $\mathcal{B}_a$.

We proceed with our exact comparison for the $q = 2$ Ising case and start by recalling the situation for the square lattice [13]. The locus $\mathcal{B}_u$ for the square lattice consists of the well-known union of circles $|u-1| = \sqrt{2}$ and $|u+1| = \sqrt{2}$.[3] The procedure for transforming the locus $\mathcal{B}_u$ found for the infinite-length, width $L_y = 2$ strip in [13] (see Fig. 20) involves two main steps. First, one retracts each of the curves going through the origin $u = 0$ so that they no longer pass through this point. It is clear that this retracting is necessary not just for $q = 2$ but for the general q-state Potts ferromagnet since the (reduced) free energy and magnetization of this model are analytic in the neighborhood of $u = 0$, i.e., they have low-temperature series expansions a finite radius of convergence. Given the inversion symmetry $\mathcal{B}_u = \mathcal{B}_a$ that holds for the square lattice and strips of this lattice (but not for the triangular lattice), this retracting means that the curves are also pulled back from the origin of the a plane. The second step in the procedure is to incorporate the feature that the 2D Potts ferromagnet has a finite-temperature phase transition. To build in this feature, one takes the two complex-conjugate ends of the curves with $Re(u)$ small and positive that have been pulled back from the origin $u = 0$ and connects them so that they cross the positive real u axis at a point u_{PM-FM} in the interval $0 < u < 1$; by the inversion symmetry this has the effect of connecting the two other ends in the $Re(u) > 0$ half plane and having them cross the real axis at $u_{PM-AFM} = u_{PM-FM}^{-1}$. The third step is to build in the feature [39, 52, 55] that if a lattice has an even coordination number, then the Ising model boundary $\mathcal{B}_u$ is symmetric under $u \to -u$; in the present case, the locus $\mathcal{B}_u$ for the $L_y = 2$ strip does not have this property because the coordination number of the vertices on the strip is 3, while the locus $\mathcal{B}_u$ for the square lattice does have the property. We thus connect the curves in the left-hand half plane $Re(u) < 0$ in such a way

[3] In Refs. [39, 52] the variable $z = e^{-2K_{Ising}} \equiv e^{-K_{Potts}}$ was used for what we denote as u here and the variable u was used for $e^{-4K_{Ising}} \equiv e^{-2K_{Potts}}$, i.e. for what would be denoted u^2 here. Thus, the circles $|u \pm 1| = \sqrt{2}$ map to the limaçon of Pascal in the u^2 plane [39].

as to have this property. As discussed in [13], the intersection points at $u = \pm i$ are the same for both the strip and the square lattice, and, indeed, on wider strips. Evidently, each step of this procedure is based on fundamental principles, and, as long as one limits oneself to obtaining the qualitative features of the locus $\mathcal{B}_u$ for the 2D case from the $L_y = 2$ strip, nothing is *ad hoc*. Of course, one cannot predict the actual values of the critical point $u_{PM-FM} = u_{PM-AFM}^{-1}$, but this is was not the goal; there are powerful ways of determining the critical point via series analyses even in cases where a spin model cannot be solved exactly in 2D. (Note that for the purpose of obtaining information about $\mathcal{B}_u$ for a model in 2D, it can be advantageous to use strips with width $L_y = 2$ rather than wider strips, since the locus $\mathcal{B}_u$ becomes progressively more complicated as L_y increases, with more curves passing through $u = 0$ [13].)

Next, we demonstrate the corresponding comparison with the locus $\mathcal{B}_u$ for the $q = 2$ Ising special case of our new results for the Potts model on the $L_y = 2$ strip of the triangular lattice and $\mathcal{B}_u$ for the model on the full 2D triangular lattice. Our calculations are shown in Figs. 15 and 16. For the Ising model on the full 2D triangular lattice, $\mathcal{B}_u$ consists of the union of an oval curve that crosses the real (imaginary) u axis at $\pm i$ with the line segment $1/\sqrt{3} \le Im(u) < \infty$ and its complex conjugate on the imaginary u axis [52]. Note that, just as was true in the case of the square strips and square lattice (and the honeycomb lattice [52]), the locus $\mathcal{B}_u$ for the Ising model on both the current strip and the full 2D triangular lattice has intersection points at $u = \pm i$. (In terms of the variable denoted u^2 in our current notation (and u in the notation of [52]), the Ising locus for the triangular lattice is the union of the semi-infinite line segment $-\infty < u^2 < -1$ and the circle $|u^2 + (1/3)| = 2/3$, and the above two intersection points map to the single intersection point at $u^2 = -1$.) Following the same procedure as for the square strip, the first step is to pull back each of the curves (of which there are now six rather than four) from the origin. On the imaginary axis, this retracting produces two complex-conjugate semi-infinite line segments, while for the other four curves, it allows one to connect them smoothly, via step 2, to form the oval. Step 3 is not necessary here since both the cyclic $L_y = 2$ strip of the triangular lattice and the full triangular lattice have the property that each vertex has even coordination number ($\Delta = 4$ for the strip and $\Delta = 6$ for the 2D lattice) so that $\mathcal{B}_u$ is invariant under the replacement $u \to -u$ [52, 55].

It is also interesting to observe that the similarities between the Ising model on the current strip and on the full 2D lattice are much stronger for the antiferromagnet than for the ferromagnet. In contrast to the case of the Ising ferromagnet, which has a finite-temperature critical point on 2D lattices but only a zero-temperature critical point on 1D and quasi-1D lattices, the Ising antiferromagnet has a zero-temperature critical point on both the full 2D triangular lattice [44] and on the infinite-length, width $L_y = 2$ strip of the triangular lattice, as a consequence of the frustration in this model. Thus in this case, there are not just similarities in the complex-temperature properties of the model, but in the actual physical thermodynamics also. Concerning the complex-temperature phase diagram, in the vicinity of this zero-temperature critical point, for the full 2D triangular lattice, $\mathcal{B}_a$ is just the inverse image of the locus $\mathcal{B}_u$ given above, namely the union of an oval intersecting the real (imaginary) a axes at $\pm\sqrt{3}$ and $\pm i$, and a finite line segment on the imaginary axis stretching from $a = -\sqrt{3}i$ to $a = \sqrt{3}i$. In the neighborhood of the origin, $a = 0$, the locus $\mathcal{B}_a$ for the present strip is exactly the same, as can be seen in Fig. 16.

Having shown the correspondences between the complex-temperature boundaries $\mathcal{B}_u$ and the associated complex-temperature phase diagrams for the exactly solved Ising case, we now use this result as a tool to suggest features of $\mathcal{B}$ for the 2D Potts model for other values of q, where it has not been exactly solved. Since the complex-temperature zeros have usually been presented in the a plane, we follow this convention here. The case $q = 3$ on strips of the square lattice and on the full square lattice was discussed in [13]. In

Figs. 21 and 22 we show $\mathcal{B}_u$ and $\mathcal{B}_a$ for the $L_y = 2$ strip of the square lattice. First, the fact that $\mathcal{B}_a$ crosses the real axis at $a = -2$ for the strip is the same as is true for the square lattice [13]; in the latter case, this follows from the existence of the zero-temperature critical point for the $q = 3$ antiferromagnet, the resultant fact that the singular locus $\mathcal{B}_a$ passes through $a = 0$, and the duality of the model, according to which if a point a is on $\mathcal{B}_a$, then the dual image $a_d = (q + a - 1)/(a - 1)$ is also on $\mathcal{B}_a$. Second, the existence of the intersection points at $a = e^{\pm 2\pi i/3}$ on $\mathcal{B}_a$ for the strip suggests that these also occur on $\mathcal{B}_a$ for the square lattice. We now extend these two comments to explore the global structure of $\mathcal{B}_a$. Since we know that the 2D $q = 3$ Potts model on the square lattice is analytic in the neighborhood of the $T = 0$ ferromagnetic point $u = 0$, our first step is to pull back the four curves that pass through $u = 0$ in Fig. 21 (equivalently, off to infinity in Fig. 22). Since we know that the 2D model has a finite-temperature critical point (the exact value, $a = 1|sqrt3$ is not crucial here), we connect the two ends of the curves in the $Re(a) > 0$ half-plane together in Fig. 22 so that they cross the positive real a plane, making the ferromagnetic critical point $a_{PM-FM} > 1$. The ends of the two curves pointing in the upper left and lower left directions in the $Re(a) < 0$ half-plane are left as is, in accordance with the finding from series analyses [49] that there are such singularities at $a_e = -1.71(1) \pm 1.46(q)i$, consistent with lying on endpoints of curves on $\mathcal{B}_a$. Since we know that the $q = 3$ Potts antiferromagnet has a $T = 0$ critical point on the square lattice, and hence $\mathcal{B}_a$ passes through $a = 0$, we move the four curves that pass through the point $a = -1/2$ (forming an intersection point) over to the right, so that at least one branch passes through $a = 0$; the exact solution for the strip suggests that $\mathcal{B}_a$ for the square lattice may also have an intersection (multiple) point at $a = 0$. The complex-temperature zeros for the $q = 3$ Potts model that have been calculated for patches of the square lattice [45, 46, 48, 49] are consistent with this suggestion (see, e.g., Fig. 1 of [49]). A third suggestion is that the intersection points on $\mathcal{B}_a$ at $a \simeq -1.85 \pm 0.85i$ for the strip have analogues on the locus $\mathcal{B}_a$ for the full square lattice. This suggestion is consistent with the patterns of complex-temperature zeros that have been calculated for patches of the square lattice, but the scatter is too great to provide a strong test.

We next use our new results on the $q = 3$ Potts model on the $L_y = 2$ strip of the triangular lattice.

3.6 Thermodynamics of the Potts Model on the $L_y = 2$ Strip of the Triangular Lattice

3.6.1 Ferromagnetic Case

The Potts ferromagnet (with real $q > 0$) on an arbitrary graph has $v > 0$ so, as is clear from eq. (1.5), the partition function satisfies the constraint of positivity. In contrast, the specific heat C is positive for the model on the (infinite-length limit of the) $L_y = 2$ triangular strip is positive if and only if $q > 1$ (for any choice of longitudinal boundary conditions). For $q = 1$, $f_{nq} = 2 \ln a = 2K$ and C vanishes identically. Since a negative specific heat is unphysical, we therefore restrict to real $q \geq 1$. For general q in this range, the reduced free energy is given for all temperatures by $f = (1/2) \ln \lambda_{S,1}$ as in (2.12) (independent of the different longitudinal boundary conditions, as must be true for the thermodynamic limit to exist). Recall that $\lambda_{S,1} \equiv \lambda_{L,5}$. It is straightforward to obtain the internal energy U and specific heat from this free energy; since the expressions are somewhat complicated, we do not list them here. We show a plot of the specific heat (with $k_B = 1$) in Fig. 23. One can observe that the value of the maximum is a monotonically increasing function of q.

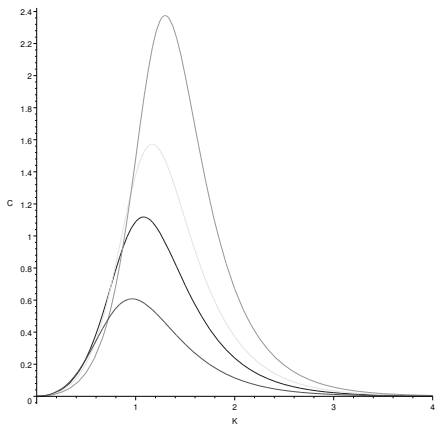

Figure 23: Specific heat (with $k_B \equiv 1$) for the Potts ferromagnet on the infinite-length, width $L_y = 2$ strip of the triangular lattice, as a function of $K = J/(k_B T)$. Going from bottom to top in order of the heights of the maxima, the curves are for $q = 2, 3, 4, 6$.

The high-temperature expansion of U is

$$U = -\frac{2J}{q}\left[1 + \frac{(q-1)}{q}K + O(K^2)\right] . \tag{3.6.1}$$

For the specific heat we have

$$C = \frac{2k_B(q-1)K^2}{q^2}\left[1 + \frac{(q+1)}{q}K + O(K^2)\right] . \tag{3.6.2}$$

The low-temperature expansions ($K \to \infty$) are

$$U = J\left[-2 + (q-1)e^{-3K}\left[3 + 4e^{-K} + 5(q-1)e^{-2K} + O(e^{-3K})\right]\right] \quad \text{as} \quad K \to \infty \tag{3.6.3}$$

and

$$C = 9k_B K^2 (q-1)e^{-3K}\left[1 + \frac{16}{9}e^{-K} + \frac{25}{9}(q-1)e^{-2K} + O(e^{-3K})\right] \quad \text{as} \quad K \to \infty \tag{3.6.4}$$

In general, the ratio ρ of the largest subdominant to the dominant λ_j's determines the asymptotic decay of the connected spin-spin correlation function and hence the correlation length

$$\xi = -\frac{1}{\ln \rho} \tag{3.6.5}$$

Since $\lambda_{L,5}$ and $\lambda_{L,2}$ are the dominant and leading subdominant λ_j's, respectively, we have

$$\rho_{FM} = \frac{\lambda_{L,2}}{\lambda_{L,5}} \tag{3.6.6}$$

and hence for the ferromagnetic zero-temperature critical point we find that the correlation length diverges, as $T \to 0$, as

$$\xi_{FM} \sim (2q)^{-1} e^{3K} , \quad \text{as} \quad K \to \infty \tag{3.6.7}$$

3.6.2 Antiferromagnetic Case

In this section we first restrict to the real range $q \geq 3$ and the additional integer value $q = 2$ (Ising case) where the Potts antiferromagnet exhibits physically acceptable behavior and then consider the remaining interval $0 < q < 3$ where (except for the trivial f_{nq} for $q = 1$) it exhibits unphysical properties. For $q \geq 3$, the free energy is given for all temperatures by (2.12), as in the ferromagnetic case but with J negative, and is the same independent of the different longitudinal boundary conditions, as is necessary for there to exist a thermodynamic limit.

We show plots of the specific heat, for several values of q, for the Potts antiferromagnet on the (infinite-length limit of the) $L_y = 2$ strip of the triangular lattice in Fig 24. In contrast to the ferromagnetic case, the maxima of C do not increase monotonically with q; they occur at 0.32 for $q = 2$ and 0.79 for $q = 3$, after which the values of the maxima decrease with increasing integral q (e.g., they are 0.45 and 0.24 for $q = 4$ and $q = 6$). The fact that the curve for C for the $q = 2$ (Ising) antiferromagnet exhibits a very broad maximum can be inferred to be a consequence of the frustration that is present in this model.

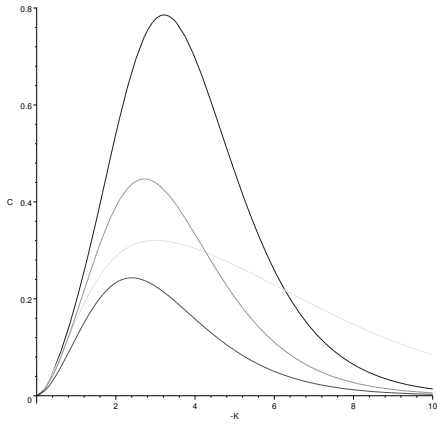

Figure 24: Specific heat (with $k_B \equiv 1$) for the Potts antiferromagnet on the infinite-length, width $L_y = 2$ strip of the triangular lattice, as a function of $-K = -J/(k_B T)$. Going downward in order of the heights of the maxima, the curves are for $q = 3, 4, 2, 6$.

The high-temperature expansions of U and C are given by (3.6.1) and (3.6.2); more generally, these expansions also apply in the range $0 < q < 3$. As discussed above, the Ising case $q = 2$ is one of the cases where one must take account of noncommutativity in the definition of the free energy and hence of thermodynamic quantities. If one sets $q = 2$ first and then takes $n \to \infty$, then $f = f_{nq} = (1/2) \ln \lambda_{L,5}|_{q=2}$ where $\lambda_{L,5}|q = 2$ was given in eq. (3.2.7), and the low-temperature expansions are

$$U_{q=2} = -\frac{J}{2}\left[1 + \frac{1}{2}e^{K/2} + \frac{23}{16}e^{3K/2} - 2e^{2K} + O(e^{5K/2})\right] \quad \text{as} \quad K \to -\infty \tag{3.6.8}$$

and

$$C_{q=2} = \frac{k_B K^2 e^{K/2}}{8}\left[1 + \frac{69}{8}e^{K} - 16e^{3K/2} + \frac{1215}{128}e^{2K} + O(e^{3K})\right] \quad \text{as} \quad K \to -\infty \, . \tag{3.6.9}$$

For the range $q \geq 3$, the low-temperature expansions are given by

$$U = \frac{(-J)e^K}{(q-2)^2}\left[(2q-3) - \frac{(2q-3)(4q-5)}{(q-2)^2}e^K + O(e^{2K})\right] \quad \text{as} \quad K \to -\infty \tag{3.6.10}$$

and

$$C = \frac{k_B K^2 e^K}{(q-2)^2}\left[(2q-3) - \frac{2(2q-3)(4q-5)}{(q-2)^2}e^K + O(e^{2K})\right] \quad \text{as} \quad K \to -\infty \ . \tag{3.6.11}$$

Note that for the antiferromagnetic case, $U(T=0) = 0$ for $q \geq 3$, but $U(T=0) = -J/2 = +|J|/2$ for $q = 2$. The vanishing value of U at $T = 0$ for $q \geq 3$ means that the Potts model can achieve its preferred ground state for this range of q, while the nonzero value of $U(T=0)$ for the Ising antiferromagnet is a consequence of the frustration that is present in this case. Similarly, the fact that the specific heat vanishes less rapidly for the Ising antiferromagnet than for the Potts model with $q \geq 3$ reflects the frustration that is present in the Ising case, which is not present for $q \geq 3$. Note that the apparent divergences that occur as $q \to 2$ in eqs. (3.6.10) and (3.6.11) are not actually reached here since these expressions apply only in the region $q \geq 3$ (the discrete integral case $q = 2$ was dealt with above).

For the zero-temperature critical points in the $q = 2$ and $q = 3$ Potts antiferromagnet,

$$\rho_{AFM,q=2,3} = \frac{\lambda_{L,2}}{\lambda_{L,5}} \tag{3.6.12}$$

Using the respective expansions (3.2.19)-(3.2.20) and (3.2.21)-(3.2.24), we find that the correlation lengths defined as in (3.6.5) diverges, as $T \to 0$, as

$$\xi_{AFM,q=2} \sim e^{-K/2} \ , \quad \text{as} \quad K \to -\infty \tag{3.6.13}$$

and

$$\xi_{AFM,q=3} \sim e^{-K} \ , \quad \text{as} \quad K \to -\infty \tag{3.6.14}$$

Next, we consider the range of real nonintegral $0 < q < 3$. The first pathology is that the Potts antiferromagnet on the infinite-length limit of the $L_y = 2$ triangular strip, defined with case of cyclic or Möbius longitudinal boundary conditions has a phase transition at the temperature $T_{p,L}$ given in eq. (3.3.7) for $0 < q < 3$ (except for f_{nq} for the integral values$q = 1, 2$), while, in contrast, if one uses free boundary conditions, then there is no phase transition at this temperature and, although there is a phase transition for $0 < q < 2$, it occurs at the temperature $T_{p,S}$ given in eq. (2.2.6), which, in general, is not equal to $T_{p,L}$. It follows that there is no well-defined thermodynamic limit for the Potts model with $0 < q < 3$ and $q \neq 1, 2$. The Ising case $q = 2$ has been dealt with in the preceding subsection. Concerning the value $q = 1$, as discussed earlier, one encounters noncommutativity in defining the free energy. If one takes $q = 1$ to start with and then $n \to \infty$, the thermodynamic limit does exist, independent of boundary conditions, and $f = f_{nq} = 2K$, $U = -2J = 2|J|$, and $C = 0$. If one starts with $q \neq 1$, takes $n \to \infty$, calculates f_{qn}, and then takes $q \to 1$, the thermodynamic limit does not exist since the result differs depending on whether one uses free longitudinal boundary conditions or cyclic (equivalently Möbius) longitudinal boundary conditions. Specifically, for this single value $q = 1$, $T_{p,S}$ is equal to $T_{p,L}$, having the value given by $k_B T_{p,S} = J/\ln[(1/2)(-1+\sqrt{5})] \simeq 2.078|J|$; in the high-temperature phase, $T > T_{p,S}$, $f_{qn} = (1/2)\ln\lambda_{L,5}$, independent of longitudinal boundary conditions, but in the low-temperature phase, $T < T_{p,S}$, the expression for f_{qn} is different for the open and cyclic (equivalently, Möbius) strips. There are also other unphysical properties, such as a negative specific heat and a negative partition function for certain ranges of temperature. These is similar to what was found for the analogous strip of the square lattice.

4 Summary

In this paper we have presented exact calculations of the partition function Z of the q-state Potts model and its generalization to real q, the Potts model, for arbitrary temperature on n-vertex strip graphs, of width $L_y = 2$, of the triangular lattice with free, cyclic, and Möbius longitudinal boundary conditions. These partition functions are equivalent to Tutte/Whitney polynomials for these graphs. The free energy is calculated exactly for the infinite-length limit of these ladder graphs and the thermodynamics is discussed. Considering the full generalization to arbitrary complex q and temperature, we determine the singular locus $\mathcal{B}$ in the corresponding $\mathbb{C}^2$ space, arising as the accumulation set of partition function zeros as $n \to \infty$. In particular, we study the connection with the $T = 0$ limit of the Potts antiferromagnet where $\mathcal{B}$ reduces to the accumulation set of chromatic zeros. Comparisons are made with our previous exact calculation of Potts model partition functions for the corresponding strips of the square lattice. Our present calculations yield, as special cases, several quantities of graph-theoretic interest, such as the number of spanning trees, spanning forests, etc., which we record.

Acknowledgment: The research of R. S. was supported in part at Stony Brook by the U. S. NSF grant PHY-97-22101 and at Brookhaven by the U.S. DOE contract DE-AC02-98CH10886.[4]

5 Appendix

5.1 General

The formulas relating the Potts model partition function $Z(G, q, v)$ and the Tutte polynomial $T(G, x, y)$ were given in [13] and hence we shall be brief here. The Tutte polynomial of G, $T(G, x, y)$, is given by [6]-[8]

$$T(G, x, y) = \sum_{G' \subseteq G} (x-1)^{k(G')-k(G)} (y-1)^{c(G')} \tag{5.1.1}$$

where $k(G')$, $e(G')$, and $n(G') = n(G)$ denote the number of components, edges, and vertices of G', and

$$c(G') = e(G') + k(G') - n(G') \tag{5.1.2}$$

is the number of independent circuits in G'. As stated in the text, $k(G) = 1$ for the graphs of interest here. Now let

$$x = 1 + \frac{q}{v} \tag{5.1.3}$$

and

$$y = a = v + 1 \tag{5.1.4}$$

so that

$$q = (x-1)(y-1) \ . \tag{5.1.5}$$

Then

$$Z(G, q, v) = (x-1)^{k(G)} (y-1)^{n(G)} T(G, x, y) \ . \tag{5.1.6}$$

For a planar graph G the Tutte polynomial satisfies the duality relation

$$T(G, x, y) = T(G^*, y, x) \tag{5.1.7}$$

[4] Accordingly, the U.S. government retains a non-exclusive royalty-free license to publish or reproduce the published form of this contribution or to allow others to do so for U.S. government purposes.

where G^* is the (planar) dual to G. As discussed in [13], the Tutte polynomial for recursively defined graphs comprised of m repetitions of some subgraph has the form

$$T(G_m, x, y) = \sum_{j=1}^{N_\lambda} c_{T,G,j} (\lambda_{T,G,j})^m \tag{5.1.8}$$

There are several special cases of the Tutte polynomial that are of interest. One that we have analyzed in the text and in previous papers is the chromatic polynomial $P(G,q)$. This is obtained by setting $y = 0$, i.e., $v = -1$, so that $x = 1 - q$; the correspondence is $P(G,q) = (-q)^{k(G)}(-1)^n T(G, 1-q, 0)$. A second special case is the flow polynomial [9, 10, 11] $F(G,q)$, obtained by setting $x = 0$ and $y = 1 - q$: $F(G,q) = (-1)^{e(G)-n(G)+k(G)} T(G, 0, 1-q)$ For planar G, given the relation (5.1.7), the flow polynomial is, up to a power of q, proportional to the chromatic polynomial: $F(G,q) \propto P(G^*, q)$. A third special case is the reliability polynomial [10], which will not be considered here.

5.2 Triangular Strip with Free Longitudinal Boundary Conditions

The generating function representation for the Tutte polynomial for the open strip of the triangular lattice comprised of $m+1$ squares with edges joining the lower-left to upper right vertices of each square, denoted S_m, is

$$\Gamma_T(S_m, x, y; z) = \sum_{m=0}^{\infty} T(S_m, x, y) z^m \ . \tag{5.2.1}$$

We have

$$\Gamma_T(S, x, y; z) = \frac{\mathcal{N}_T(S, x, y; z)}{\mathcal{D}_T(S, x, y; z)} \tag{5.2.2}$$

where

$$\mathcal{N}_T(S, x, y; z) = A_{T,S,0} + A_{T,S,1} z \tag{5.2.3}$$

with

$$A_{T,S,0} = x(x+1)^2 + 2xy + y(y+1) \tag{5.2.4}$$

$$A_{T,S,1} = -x^3 y^2 \tag{5.2.5}$$

and

$$\begin{aligned} \mathcal{D}_T(S, x, y, z) &= 1 - [(x+1)^2 + y(y+2)]z + x^2 y^2 z^2 \\ &= \prod_{j=1}^{2} (1 - \lambda_{T,S,j} z) \end{aligned} \tag{5.2.6}$$

with

$$\lambda_{T,S,(1,2)} = \frac{1}{2}\left[(x+1)^2 + y(y+2) \pm (1+x+y)\sqrt{R_T} \right] \tag{5.2.7}$$

where

$$R_T = (x+1)^2 + (y+1)^2 - 1 - 2xy \ . \tag{5.2.8}$$

The corresponding closed-form expression is given by the general formula [13]

$$T(S_m, x, y) = \left[\frac{A_{T,S,0}\lambda_{T,S,1} + A_{T,S,1}}{\lambda_{T,S,1} - \lambda_{T,S,2}} \right] (\lambda_{T,S,1})^m + \left[\frac{A_{T,S,0}\lambda_{T,S,2} + A_{T,S,1}}{\lambda_{T,S,2} - \lambda_{T,S,1}} \right] (\lambda_{T,S,2})^m \ . \tag{5.2.9}$$

It is easily checked that this is a symmetric function of the $\lambda_{S,j}$, $j = 1, 2$.

5.3 Cyclic and Möbius Strips of the Triangular Lattice

We have

$$T(L_m, x, y) = \sum_{j=1}^{6} c_{T,L,j} (\lambda_{T,L,j})^m \tag{5.3.1}$$

and

$$T(ML_m, x, y) = \sum_{j=1}^{6} c_{T,ML,j} (\lambda_{T,ML,j})^m \tag{5.3.2}$$

It is convenient to extract a common factor from the coefficients:

$$c_{T,G,j} \equiv \frac{\bar{c}_{T,G,j}}{x-1} \ , \quad G = L, ML \ . \tag{5.3.3}$$

Of course, although the individual terms contributing to the Tutte polynomial are thus rational functions of x rather than polynomials in x, the full Tutte polynomial is a polynomial in both x and y. We have

$$\lambda_{T,ML,j} = \lambda_{T,L,j} \ , \quad j = 1, ..., 6 \tag{5.3.4}$$

$$\lambda_{T,L,1} = 1 \tag{5.3.5}$$

and

$$\lambda_{T,5} = \lambda_{T,S,1} \ , \quad \lambda_{T,6} = \lambda_{T,S,2} \tag{5.3.6}$$

where $\lambda_{T,S,1}$ and $\lambda_{T,S,2}$ were given in eq. (5.2.7) with (5.2.8). The $\lambda_{T,L,j}$, $j = 2, 3, 4$, are solutions of the cubic equation

$$\xi^3 - (3 + 2x + 2y + y^2)\xi^2 + [(x+1)^2 + 2xy(y+1)]\xi - x^2 y^2 = 0 \tag{5.3.7}$$

We label these $\lambda_{T,L,j}$'s in a manner corresponding to the $\lambda_{L,j}$'s occurring in the Potts model partition function, so that $\lambda_{T,L,5}$ is dominant in the region in (x, y) equivalent to the PM phase, and so forth for the others. We note that

$$\lambda_{T,L,2}\lambda_{T,L,3}\lambda_{T,L,4} = \lambda_{T,L,5}\lambda_{T,L,6} = x^2 y^2 \ . \tag{5.3.8}$$

The coefficients for the cyclic strip are

$$\bar{c}_{T,L,1} = [(x-1)(y-1)]^2 - 3(x-1)(y-1) + 1 \tag{5.3.9}$$

$$\bar{c}_{T,L,j} = xy - x - y \quad \text{for} \quad j = 2, 3, 4 \tag{5.3.10}$$

and

$$\bar{c}_{T,L,j} = 1 \quad \text{for} \quad j = 5, 6 \ . \tag{5.3.11}$$

These are symmetric under interchange of $x \leftrightarrow y$, which is a consequence of the fact that the $\bar{c}_{L,j}$ are functions only of q, which, by eq. (5.1.5) is a symmetric function of x and y. For the Möbius strip, we find

$$\bar{c}_{T,ML,1} = -1 \tag{5.3.12}$$

and

$$\bar{c}_{T,ML,5} = \bar{c}_{T,ML,6} = 1 \ . \tag{5.3.13}$$

The $c_{T,ML,j}$, $j = 2, 3, 4$ can be calculated from the generating function using the formula given in [13]. Their form is more complicated, as is evident from the results given in [32] for the corresponding chromatic polynomial for this case. We write the generating function as

$$\Gamma_T(ML, x, y, z) = \sum_{m=1}^{\infty} T(ML_m, x, y) z^{m-1} \ . \tag{5.3.14}$$

with

$$\Gamma_T(ML, x, y, z) = \frac{\mathcal{N}_T(ML, x, y, z)}{\mathcal{D}_T(ML, x, y, z)} \tag{5.3.15}$$

where

$$\mathcal{D}_T(ML, x, y, z) = \mathcal{D}_T(L, x, y, z) = \prod_{j=1}^{6} (1 - \lambda_{L,j} z) \tag{5.3.16}$$

and

$$\mathcal{N}_T(ML, x, y, z) = \sum_{j=0}^{5} A_{ML,j} z^j \tag{5.3.17}$$

with

$$A_{ML,0} = y(x + y + y^2) \tag{5.3.18}$$

$$A_{ML,1} = yx - 4y^2x - 4y^3 - 3y^4 - 5y^3x - y^5 - 2x^2y - x^3y - x^2y^2 - x^2y^3 + 2y + 2x + 3x^2 + x^3 \tag{5.3.19}$$

$$\begin{aligned} A_{ML,2} &= y(-2x^2y + 4yx + 3x + 3y + x^2y^3 - 2x^3y + 6x^2y^2 + 2xy^4 \\ &+ 4y^3x + y^4x^2 + 3x^3y^2 + 5y^2 + 3y^3 + y^4 + 6y^2x + 2x^2) \end{aligned} \tag{5.3.20}$$

$$\begin{aligned} A_{ML,3} &= -y(-2x^2y - 3yx - x - y - x^4y + 3x^2y^3 - 2x^3y + 8x^2y^2 + 2xy^4 \\ &+ 2x^3y^4 - x^3y^3 + 5y^3x - x^3 + x^4y^2 + 2y^4x^2 + 4x^3y^2 - 2y^2 \\ &- y^3 + 3y^2x - 2x^2) \end{aligned} \tag{5.3.21}$$

$$A_{ML,4} = x^2y^2(-1 + x^2y^3 - x^2y^2 - x^2 + y^2 - 2x + y + 2y^3x + x^2y + y^3 + yx) \tag{5.3.22}$$

and

$$A_{ML,5} = -y^4x^4(y - 1) \ . \tag{5.3.23}$$

5.4 Special Values of Tutte Polynomials for Strips of the Triangular Lattice

For a given graph $G = (V, E)$, at certain special values of the arguments x and y, the Tutte polynomial $T(G, x, y)$ yields quantities of basic graph-theoretic interest [8]-[11]. We recall some definitions: a spanning subgraph was defined at the beginning of the paper; a tree is a connected graph with no cycles; a forest is a graph containing one or more trees; and a spanning tree is a spanning subgraph that is a tree. We recall that the graphs G that we consider are connected. Then the number of spanning trees of G, $N_{ST}(G)$, is

$$N_{ST}(G) = T(G, 1, 1) \ , \tag{5.4.1}$$

the number of spanning forests of G, $N_{SF}(G)$, is

$$N_{SF}(G) = T(G, 2, 1) \ , \tag{5.4.2}$$

the number of connected spanning subgraphs of G, $N_{CSSG}(G)$, is

$$N_{CSSG}(G) = T(G, 1, 2) \ , \tag{5.4.3}$$

and the number of spanning subgraphs of G, $N_{SSG}(G)$, is

$$N_{SSG}(G) = T(G, 2, 2) \ . \tag{5.4.4}$$

From the duality relation (5.1.7), one has, for planar graphs G and their planar duals D^*,

$$N_{ST}(G) = N_{ST}(G^*) \ , \quad N_{SSG}(G) = N_{SSG}(G^*) \tag{5.4.5}$$

and

$$N_{SF}(G) = N_{CSSG}(G^*) \ . \tag{5.4.6}$$

From our calculations of Tutte polynomials, we find that

$$N_{ST}(S_m) = N_{ST}(S_m^*) = \left(4 + \frac{9\sqrt{5}}{5}\right)\left(\frac{7+3\sqrt{5}}{2}\right)^m + \left(4 - \frac{9\sqrt{5}}{5}\right)\left(\frac{7-3\sqrt{5}}{2}\right)^m \tag{5.4.7}$$

$$N_{SF}(S_m) = N_{CSSG}(S_m^*) = \left(12 + \frac{17\sqrt{2}}{2}\right)\left[2(3+2\sqrt{2})\right]^m + \left(12 - \frac{17\sqrt{2}}{2}\right)\left[2(3-2\sqrt{2})\right]^m \tag{5.4.8}$$

$$N_{CSSG}(S_m) = N_{SF}(S_m^*) = (7+5\sqrt{2})\left[2(3+2\sqrt{2})\right]^m + (7-5\sqrt{2})\left[2(3-2\sqrt{2})\right]^m \tag{5.4.9}$$

$$N_{SSG}(S_m) = N_{SSG}(S_m^*) = 2^{4m+5} \ . \tag{5.4.10}$$

For the cyclic $L_y = 2$ strip of the triangular lattice, L_m, we first note that for $m \geq 3$, L_m is a (proper) graph, but for $m = 1$ and $m = 2$, L_m is not a proper graph, but instead, is a multigraph, with multiple edges (and, for $m = 1$, loops). The following formulas apply for all $m \geq 1$:

$$N_{ST}(L_m) = N_{ST}(L_m^*) = \frac{2m}{5}\left[\left(\frac{7+3\sqrt{5}}{2}\right)^m + \left(\frac{7-3\sqrt{5}}{2}\right)^m - 2\right] \tag{5.4.11}$$

$$N_{SF}(L_m) = N_{CSSG}(L_m^*) = 1 - \sum_{j=2,3,4} (\lambda_{T,j})^m + \left[2(3+2\sqrt{2}\,)\right]^m + \left[2(3-2\sqrt{2}\,)\right]^m \,. \tag{5.4.12}$$

where $\lambda_{T,L,j}$, $j = 2, 3, 4$ are the roots of eq. (5.3.7) for $x = 2, y = 1$, viz., $\xi^3 - 10\xi^2 + 17\xi - 4 = 0$:

$$\lambda_{T,L,2}(x = 2, y = 1) = 0.280176... \tag{5.4.13}$$

$$\lambda_{T,L,3}(x = 2, y = 1) = 1.803442... \tag{5.4.14}$$

$$\lambda_{T,L,4}(x = 2, y = 1) = 7.916382... \tag{5.4.15}$$

We also calculate

$$\begin{aligned} N_{CSSG}(L_m) = N_{SF}(L_m^*) &= -(2 + \frac{6m}{7}) + \left[1 + m\frac{(3-\sqrt{2}\,)}{7}\right]\left[2(3+2\sqrt{2}\,)\right]^m \\ &+ \left[1 + m\frac{(3+\sqrt{2}\,)}{7}\,\right]\left[2(3-2\sqrt{2}\,)\right]^m \end{aligned} \tag{5.4.16}$$

$$N_{SSG}(L_m) = N_{SSG}(L_m^*) = 2^{4m} \,. \tag{5.4.17}$$

Since $T(G_m, x, y)$ grows exponentially as $m \to \infty$ for the families $G_m = S_m$ and L_m for $(x, y) = (1, 1)$, (2,1), (1,2), and (2,2), one defines the corresponding constants

$$z_{set}(\{G\}) = \lim_{n(G)\to\infty} n(G)^{-1} \ln N_{set}(G) \;, \quad set = ST,\ SF,\ CSSG,\ SSG \tag{5.4.18}$$

where, as above, the symbol $\{G\}$ denotes the limit of the graph family G as $n(G) \to \infty$ (and the z here should not be confused with the auxiliary expansion variable in the generating function (5.2.1) or the Potts partition function $Z(G, q, v)$.) General inequalities for these were given in [13]. Our results yield

$$z_{ST}(\{G\}) = \frac{1}{2}\ln\left(\frac{7+3\sqrt{5}}{2}\right) \simeq 0.962424 \quad \text{for} \quad G = S, L, ML \tag{5.4.19}$$

$$z_{SF}(\{G\}) = z_{CSSG}(\{G\}) = \frac{1}{2}\ln[2(3+2\sqrt{2})] \simeq 1.22795 \quad \text{for} \quad G = S, L, ML \tag{5.4.20}$$

and

$$z_{SSG}(\{G\}) = 2\ln 2 \simeq 1.38629 \quad \text{for} \quad G = S, L, ML \tag{5.4.21}$$

The cyclic $L_y = 2$ strip of the triangular lattice is a κ-regular graph [5] with $\kappa = 4$. It is therefore of interest to compare the value of z_{ST} that we have obtained for the $n \to \infty$ limit of this family with an upper bound for κ-regular graphs with $\kappa \ge 3$ [57, 58] , viz.

$$z_{ST}(\{G\}) \le z_{ST,u.b.}(\{G\}) \;, \quad \text{where} \quad z_{ST,u.b.}(\{G\}) = \ln\left[\frac{(\kappa-1)^{\kappa-1}}{[\kappa(\kappa-2)]^{(\kappa/2)-1}}\right] \tag{5.4.22}$$

For this purpose we define r as the ratio of the left- to the right-hand side of eq. (5.4.22). We have

$$r_{ST}(\{L\}) = \frac{\frac{1}{2}\ln\left(\frac{7+3\sqrt{5}}{2}\right)}{3\ln\left(\frac{3}{2}\right)} \simeq 0.791 \tag{5.4.23}$$

[5] A κ-regular graph is a graph in which all of the vertices have the same degree, κ.

Another comparison of interest is the ratio of z_{ST} for these $L_y = 2$ strips with z_{ST} for the full 2D triangular lattice, which has the value [56]

$$z_{ST,tri} = 2z_{hc} = \frac{3\sqrt{3}}{\pi}(1 - 5^{-2} + 7^{-2} - 11^{-2} + 13^{-2} - ...) = 1.615329736... \tag{5.4.24}$$

$$\frac{z_{ST}(\{L\})}{z_{ST}(tri)} \simeq 0.596 \tag{5.4.25}$$

Finally, we may also compare the z values above with those for the infinite-length limit of the $L_y = 2$ strip of the square lattice (with free transverse boundary conditions). This is [59, 60, 13]

$$z_{ST} = \frac{1}{2}\ln(2 + \sqrt{3}\ ) \simeq 0.658479 \tag{5.4.26}$$

Further, the calculation of the Tutte polynomial for the open and/or cyclic $L_y = 2$ strip of the square lattice [13] yields

$$z_{SF} = \frac{1}{2}\ln[2(2 + \sqrt{3}\ )] \simeq 1.00505 \tag{5.4.27}$$

$$z_{CSSG} = \frac{1}{2}\ln\Big(\frac{5 + \sqrt{17}}{2}\Big) \simeq 0.758832 \tag{5.4.28}$$

$$z_{SSG} = \frac{3}{2}\ln 2 = 1.03972 \tag{5.4.29}$$

Thus, one observes that each of these four quantities is greater for the (infinite-length limit of the) $L_y = 2$ strip of the triangular lattice than for the (same limit of the) $L_y = 2$ strip of the square lattice. For z_{ST}, this follows from the fact that one can obtain the strip of the triangular lattice from that for the square lattice by uniformly adding a diagonal bond to each of the squares [61]. The inequalities for the other quantities z_{SF}, z_{CSSG}, and z_{SSG} are presumably a consequence of this fact also.

5.5 Tutte Polynomials for Dual Graphs

Since the Tutte polynomial satisfies the duality relation (5.1.7) for a planar graph G, our calculations of the Tutte polynomials $T(G_m, x, y)$ for the open and cyclic $L_y = 2$ strips of the triangular lattice, S_m and L_m, also yield the corresponding Tutte polynomials for the duals of these graphs. For $m \geq 3$, the dual of L_m is a graph with $n = 2m + 2$ vertices comprised of the circuit graph C_{2m} together with two additional vertices, which we denote v_e and v_o such that, if we label the vertices on C_{2m} as v_j, $j = 1, .., 2m$, then each of the v_j with j even is connected by an edges to v_e and each of the v_j with j odd is connected to v_o. We shall denote this graph as an "alternating wheel", A_{2m+2}. Then

$$T(A_{2m+2}, x, y) = T(L_m, y, x)\ , \quad \text{for} \quad m \geq 3 \tag{5.5.1}$$

The cases $m = 1$ and $m = 2$ can be dealt with in a similar manner.

The dual of the open strip graph S_m is the multigraph formed by a line of $2(m + 1)$ vertices, of which the interior $2m$ vertices are connected by single edges to a single additional vertex, and the two end vertices on the line are connected to this additional vertex by double edges. We have $T((S_m)^*, x, y) = T(S_m, y, x)$.

References

[1] R. B. Potts, Proc. Camb. Phil. Soc. **48** 106 (1952).

[2] F. Y. Wu, Rev. Mod. Phys. **54** (1982) 235.

[3] G. D. Birkhoff, Ann. of Math. **14** (1912) 42.

[4] H. Whitney, Ann. of Math. **33** (1932) 688.

[5] P. W. Kasteleyn and C. M. Fortuin, J. Phys. Soc. Jpn. **26** (1969) (Suppl.) 11; C. M. Fortuin and P. W. Kasteleyn, Physica **57** (1972) 536.

[6] W. T. Tutte, Can. J. Math. **6** (1954) 80.

[7] W. T. Tutte, J. Combin. Theory **2** (1967) 301.

[8] W. T. Tutte, "Chromials", in Lecture Notes in Math. v. 411 (1974) 243; *Graph Theory*, vol. 21 of Encyclopedia of Mathematics and Applications (Addison-Wesley, Menlo Park, 1984).

[9] N. L. Biggs, *Algebraic Graph Theory* (2nd ed., Cambridge Univ. Press, Cambridge, 1993).

[10] D. J. A. Welsh, *Complexity: Knots, Colourings, and Counting*, London Math. Soc. Lect. Note Ser. 186 (Cambridge University Press, Cambridge, 1993).

[11] B. Bollobás, *Modern Graph Theory* (Springer, New York, 1998).

[12] R. Shrock, in the *Proceedings of the 1999 British Combinatorial Conference, BCC99* (July, 1999), Discrete Math., to appear.

[13] R. Shrock, Physica A, in press.

[14] S.-C. Chang and R. Shrock, Stony Brook preprints YITP-SB-99-50,58.

[15] R. C. Read, J. Combin. Theory **4** (1968) 52.

[16] R. C. Read and W. T. Tutte, "Chromatic Polynomials", in *Selected Topics in Graph Theory, 3*, eds. L. W. Beineke and R. J. Wilson (Academic Press, New York, 1988.).

[17] R. Shrock and S.-H. Tsai, Phys. Rev. **E55** (1997) 5165.

[18] N. L. Biggs, R. M. Damerell, and D. A. Sands, J. Combin. Theory B **12** (1972) 123.

[19] N. L. Biggs and G. H. Meredith, J. Combin. Theory B**20** (1976) 5; N. L. Biggs, Bull. London Math. Soc. **9** (1976) 54.

[20] S. Beraha, J. Kahane, and N. Weiss, J. Combin. Theory B **27** (1979) 1; *ibid.* **28** (1980) 52.

[21] R. C. Read, in Proc. 3rd Caribbean Conf. on Combin. and Computing (1981); Proc. 5th Caribbean Conf. on Combin. and Computing (1988).

[22] R. J. Baxter, J. Phys. A **20** (1987) 5241.

[23] R. C. Read and G. F. Royle, in *Graph Theory, Combinatorics, and Applications* (Wiley, NY, 1991), vol. 2, p. 1009.

[24] R. Shrock and S.-H. Tsai, Phys. Rev. **E56** (1997) 1342, 2733, 3935, 4111.

[25] R. Shrock and S.-H. Tsai, Phys. Rev. **E58** (1998) 4332; cond-mat/9808057.

[26] M. Roček, R. Shrock, and S.-H. Tsai, Physica **A252** (1998) 505.

[27] M. Roček, R. Shrock, and S.-H. Tsai, Physica **A259** (1998) 367.

[28] R. Shrock and S.-H. Tsai, Physica **A259** (1998) 315.

[29] R. Shrock and S.-H. Tsai, J. Phys. A **31** (1998) 9641; Physica **A265** (1999) 186.

[30] R. Shrock and S.-H. Tsai, J. Phys. A Lett. **32** (1999) L195.

[31] R. Shrock and S.-H. Tsai, Phys. Rev. **E60** (1999) 3512.

[32] R. Shrock and S.-H. Tsai, Physica A **275** (1999) 429.

[33] A. Sokal, Combin. Prob. Comput., in press (cond-mat/9904146); cond-mat/9910503.

[34] R. Shrock and S.-H. Tsai, J. Phys. **32** (1999) 5053.

[35] N. L. Biggs, LSE report LSE-CDAM-99-03 (May 1999), to appear.

[36] R. Shrock, Phys. Lett. **A261** (1999) 57.

[37] N. L. Biggs and R. Shrock, J. Phys. A (Letts) **32**, L489 (1999).

[38] H. Kluepfel and R. Shrock, YITP-99-32; H. Kluepfel, Stony Brook thesis (July, 1999).

[39] V. Matveev and R. Shrock, J. Phys. A **28** (1995) 1557.

[40] J. V. Uspensky, *Theory of Equations* (McGraw-Hill, NY 1948), 264.

[41] J. Salas and A. Sokal, J. Stat. Phys. **86** (1997) 551.

[42] R. Shrock and S.-H. Tsai, Phys. Rev. **55**, 5184 (1997).

[43] R. Hartshorne, *Algebraic Geometry* (Springer, New York, 1977).

[44] G. H. Wannier, Phys. Rev. **79**, 357 (1950); J. Stephenson, J. Math. Phys. **5**, 1009 (1964).

[45] P. P. Martin and J. M. Maillard, J. Phys. A **19** (1986) L547.

[46] P. P. Martin, *Potts Models and Related Problems in Statistical Mechanics* (World Scientific, Singapore, 1991).

[47] C. N. Chen, C. K. Hu, and F. Y. Wu, Phys. Rev. Lett. **76** (1996) 169.

[48] F. Y. Wu, G. Rollet, H. Y. Huang, J. M. Maillard, C. K. Hu, and C. N. Chen, Phys. Rev. Lett. **76** (1996) 173.

[49] V. Matveev and R. Shrock, Phys. Rev. **E54** (1996) 6174.

[50] H. Feldmann, R. Shrock, and S.-H. Tsai, J. Phys. A (Lett.) **30** (1997) L663; Phys. Rev. **E57** (1998) 1335.

[51] H. Feldmann, A. J. Guttmann, I. Jensen, R. Shrock, and S.-H. Tsai), J. Phys. A **31** (1998) 2287.

[52] V. Matveev and R. Shrock, J. Phys. A **29** (1996) 803.

[53] V. Matveev and R. Shrock, J. Phys. A (Letts.) **28** (1995) L533.

[54] V. Matveev and R. Shrock, Phys. Lett. **A204** (1995) 353.

[55] V. Matveev and R. Shrock, J. Phys. A **28** (1995) 5235.

[56] F. Y. Wu, J. Phys. A **10** (1977) L113.

[57] B. McKay, J. Combinatorics **4** (1983) 149.

[58] F. Chung and S.-T. Yau, www.combinatorics.org R12, 6 (1999).

[59] R. K. Guy and F. Harary, Univ. of Calgary Rept. 2, 1966; J. Sedlácek, in Combinatorial Structures and Applications (Gordon and Breach, New York, 1970), p. 387.

[60] W. J. Tzeng and F. Y. Wu, Lett. Appl. Math. to appear (cond-mat/0001408).

[61] R. Shrock and F. Y. Wu, Northeastern - Stony Brook preprint.